

Frequency moments for two-spin light scattering in antiferromagnets*

W. J. Brya and Peter M. Richards

Sandia Laboratories, Albuquerque, New Mexico 87115

(Received 11 May 1973; revised manuscript received 26 October 1973)

The low-order frequency moments for two-spin light scattering in antiferromagnets are calculated in terms of static multispin correlations and compared with experimental data in MnF_2 , NiF_2 , and RbMnF_3 . Expressions for the integrated scattering intensity A (the zeroth moment) and the first moment $\langle\omega\rangle$ over the full temperature range ($0 \leq T \leq \infty$) are obtained. These can be evaluated exactly in the limits of infinite temperature and of zero temperature, within the spin-wave formalism. For intermediate temperatures, suitable approximations are made. In the paramagnetic phase, the multispin correlations are decoupled into products of two-spin correlations which are evaluated using recently published results for pair correlations in Heisenberg ferromagnets. In the ordered state, A and $\langle\omega\rangle$ are estimated using the molecular-field formalism, but modified to include the effects of short-range fluctuations. Exact expressions for the second moment $\langle\omega^2\rangle$ in the infinite-temperature limit are also derived. In MnF_2 the intensity increases with increasing T , in qualitative agreement with theory, although an anomalous, unexplained increase is observed in the paramagnetic state. The first moment $\langle\omega\rangle$ decreases with increasing T and shows critical-type behavior near the Néel temperature T_N ; in the paramagnetic state the agreement between experiment and theory is very good, especially at T_N where the observed $\langle\omega\rangle = 17 \text{ cm}^{-1}$ is to be compared with the theoretical value of 15 cm^{-1} . The observed high-temperature $\langle\omega^2\rangle$ are also in reasonable accord with theory. Detailed comparison is made between theory and experiment for $\langle\omega\rangle$ in the zero temperature limit in MnF_2 , NiF_2 , and RbMnF_3 . The implications of these results for studies of the dynamics of short-range spin correlations and for a determination of the spin-system parameters are discussed.

I. INTRODUCTION

The Raman scattering of light by two-magnon excitations in antiferromagnets has been of considerable experimental and theoretical interest in recent years. Extensive experimental data on two-magnon scattering in a number of diverse systems have been accumulated in the few years since the first observations^{1,2} of the effect in MnF_2 and FeF_2 . At the lowest temperatures, one observes a well-defined asymmetric line at about twice the maximum zone-boundary magnon energy. As the temperature increases, the peak in the scattering profile decreases in energy, the linewidth increases, and the spectrum shows an *apparent* decrease in intensity. In a number of the systems,^{3,4} the spectrum is observed to persist to temperatures well above the Néel temperature T_N , showing a broad featureless line with a small nonzero energy shift.

The theoretical description^{2,5-7} of the scattering process is based on a spin-photon interaction which causes simultaneous spin deviations on adjacent antiferromagnetically coupled spin sites. Using this interaction, Elliott *et al.*⁶ and Elliott and Thorpe⁷ developed a Green's-function theory for two-magnon scattering and applied it at zero temperature. Their decoupling scheme, which is used to evaluate the time-dependent four-spin correlation function that characterizes the scattering profile, explicitly includes the effects of magnon-mag-

non interactions which occur because of the creation of magnons on adjacent spin sites. In general, their predictions for the position and shape of the scattering profile have been in excellent agreement with experiment.

Unfortunately, this and similar theories⁸⁻¹³ have been less successful in explaining the observed scattering spectra at higher temperatures, particularly in the region of T_N and above. The difficulty arises primarily from the inability to evaluate reliably the time-dependent four-spin correlation function as a function of temperature. Within the Green's-function formalism, various authors¹¹⁻¹³ have estimated the behavior of this correlation in the spin-wave region. They obtain reasonable agreement for the position of the scattering peak to temperatures $T \sim 0.8 T_N$, but the predicted linewidth is typically less than is observed. Equations of motion and random-phase-approximation decouplings have also been used in the paramagnetic phase.^{9,10} Kawasaki⁹ obtained a general expression for the line shape which agrees quite well; however, he used both frequency and peak intensity as adjustable scale parameters at each temperature and thus made no serious attempt to compare temperature variation of the peak frequency or intensity. In fact, his estimates of a 60% decrease of the peak frequency in NiF_2 between $T=0$ and T_N and a total intensity which decreases as temperature increases are not in agreement with the ob-

served³ 20% decrease and (as reported here) increase of total intensity with increasing temperature. S6lyom¹⁰ confined his treatment above T_N to renormalization of the zone-boundary magnon energy and obtained good agreement with the observed 20% figure in NiF_2 . Since his theory contained no damping effects he could not discuss line-width or intensity of the scattering profile, and his peak excitation energy did not go to zero at $T = \infty$. The work of Pershan and Oseroff⁸ which relates the peak frequency to the magnetic heat capacity is quite successful below T_N but considerably underestimates the renormalization above T_N .

Recently, we reported^{14,15} briefly on comprehensive experiments and theory for two-spin fluctuation light scattering in MnF_2 from well below to well above T_N ; a similar study¹⁶ in the canted antiferromagnet NiF_2 has also been conducted. The analysis of the scattering profile is novel in that it is based on the frequency moments and integrated intensity of the spectrum. The moments and intensity are useful quantities to measure since they involve static correlations which can usually be calculated with reasonable reliability; in particular, one can now obtain useful expressions for the scattering behavior in the paramagnetic state for direct comparison with experiment. A calculation of the overall line shape, on the other hand, typically requires the decoupling of dynamical equations.

Here we present a complete detailed discussion of the theoretical formalism for the spectral moments of two-spin light scattering and compare the results with experimental data in MnF_2 . Expressions for the integrated scattering intensity and first moment over the full temperature range ($0 \leq T \leq \infty$) are obtained; the second moment in the infinite-temperature limit is also derived. In general, the results are in good agreement with the observed behavior in MnF_2 , particularly at the very lowest temperatures and, with the exception of the intensity, in the paramagnetic phase. The implications of these results for studies of the dynamics of short-range spin correlations and for the determination of spin-system parameters are considered.

II. THEORY

A. Spin-system Hamiltonians

For the two-sublattice antiferromagnet, we consider a general spin Hamiltonian of the form

$$H_0 = \frac{1}{2} \sum_{ij} J_{ij} \vec{S}_i \cdot \vec{S}_j + D \sum_i (S_i^z)^2 + \frac{1}{2} \sum_{ij} \sum_{\alpha\beta} K_{ij}^{\alpha\beta} S_i^\alpha S_j^\beta, \quad (1)$$

where i and j are summed over the N magnetic ions in the crystal and $\alpha, \beta = x, y, z$. Here, the exchange

interaction is expressed in the usual isotropic Heisenberg form with exchange constants J_{ij} . Exchange interactions between all pairs of magnetic ions are included although, in practice, they are normally only appreciable for a limited number of near neighbors. The axial single-ion anisotropy term D can be positive or negative and, in the ordered magnetic state, typically leads to an easy plane or easy axis of magnetization, respectively. The final term in Eq. (1) represents the dipolar interaction

$$K_{ij}^{\alpha\beta} = g^2 \mu_B^2 (\gamma_{ij}^2 \delta_{\alpha\beta} - 3r_{ij}^\alpha r_{ij}^\beta) / r_{ij}^5, \quad (2)$$

where \vec{r}_{ij} is the vector joining the pair $\langle ij \rangle$; this is generally a small term. In many cases, the anisotropic effect of the dipolar term and of any small anisotropic exchange which may be present will be included in an effective value for D .

The crystal structure for the rutile-structure antiferromagnets, such as MnF_2 , is shown in Fig. 1; the magnetic ions are situated on a body-centered tetragonal lattice. For MnF_2 the spins order along the crystal c axis [chosen to coincide with the z axis of Eq. (1)] at temperatures below the Néel temperature $T_N = 67.7^\circ\text{K}$. Inelastic neutron-scattering studies^{17,18} at low temperatures show that the spin-wave spectrum is adequately described by Eq. (1) if one only includes isotropic exchange interactions between three types of magnetic neighbors, as indicated in Fig. 1, and the dipole-dipole interaction; the single-ion anisotropy D is negligible. The next-nearest-neighbor antiferromagnetic exchange J_2 is dominant, with the nearest-neighbor ferromagnetic J_1 about a factor of 5 smaller and the antiferromagnetic J_3 considerably weaker.

The basic interaction Hamiltonian H' for two-spin fluctuation light scattering in antiferromagnetic materials has been extensively described and developed elsewhere.^{2,5-7} The specific form for the Hamiltonian is determined by the crystal symmetry. For the rutile-structure antiferromagnets, Fleury and Loudon² have determined its characteristics in some detail and obtain, for the dominant terms,

$$H' = \frac{1}{2} \sum_{ij} \{ A(E_1^x E_2^x + E_1^y E_2^y) + B E_1^z E_2^z + C(E_1^x E_2^y + E_1^y E_2^x) \sigma_{ij}^x \sigma_{ij}^y + D[(E_1^y E_2^z + E_1^z E_2^y) \times \sigma_{ij}^y \sigma_{ij}^z + (E_1^x E_2^z + E_1^z E_2^x) \sigma_{ij}^x \sigma_{ij}^z] \} \times [\vec{S}_i \cdot \vec{S}_j + (\gamma - 1) S_i^z S_j^z]. \quad (3)$$

The coupling constants A , B , C and D for the scattering process are proportional to a ground-state-excited-state exchange interaction and are assumed to be nonzero only for the next-nearest-neighbor (nnn) ion pairs $\langle ij \rangle$ coupled by the antiferromagnetic exchange J_2 . \vec{E}_1 and \vec{E}_2 are the electric vectors for

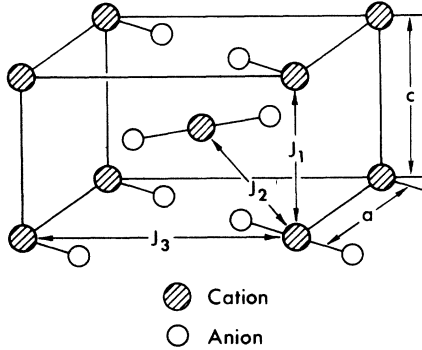


FIG. 1. Crystal structure for the rutile-structure antiferromagnets. The first three neighbor exchange interactions J_i for the magnetic cations are indicated.

the incident and scattered light waves, respectively. The σ_{ij}^α are phase factors for the nnn pairs $\langle ij \rangle$ defined by

$$\sigma_{ij}^\alpha = \text{sgn}(\vec{r}_{ij})_\alpha, \quad \alpha = x, y, z \quad (4)$$

and are equal to either +1 or -1. The quantity γ represents an anisotropy factor (for $\gamma \neq 1$) which is allowed by the tetragonal symmetry. Contributions to Eq. (3) from antisymmetric terms, which are also allowed by the crystal symmetry, have been shown experimentally² to be negligible for MnF_2 and several other rutile-structure antiferromagnets. Likewise, additional terms⁷ which may be important in pseudospin systems like CoF_2 are also omitted from Eq. (3). For our purposes, we rewrite Eq. (3) in the more manageable form

$$H' = \frac{1}{2} \sum_{\alpha\beta} \sum_{ij} G_{ij}^{\alpha\beta} [\vec{S}_i \cdot \vec{S}_j + (\gamma - 1) S_i^\alpha S_j^\alpha], \quad (5)$$

where α and β are the directions of polarization for the incident and scattered light waves. For the case $\alpha \neq \beta$, the nonzero $G_{ij}^{\alpha\beta}$ vary in sign among the eight nnn pairs and satisfy the useful relation

$$\sum_j G_{ij}^{\alpha\beta} = 0. \quad (6)$$

In previous treatments of the scattering it has been common practice to consider only the transverse components ($S_i^x S_j^x + S_i^y S_j^y$) in H' since they give the dominant contribution to the two-magnon light scattering at low temperatures. For a detailed study over the full temperature range, however, it is essential to retain the longitudinal components $S_i^z S_j^z$ as well.

$$\langle \omega^n \rangle = \int_{-\infty}^{\infty} \omega^n I(\omega) d\omega / \int_{-\infty}^{\infty} I(\omega) d\omega = (i)^n \left\langle \left(\frac{d}{dt} \right)^n H'(t) H'(0) \right\rangle_{t=0} / \langle H'(t) H'(0) \rangle_{t=0}. \quad (10)$$

The higher moments ($n \geq 1$) are normalized with respect to the integrated intensity and, as we shall

B. General procedure for moment calculations

The intensity of inelastic light scattering with frequency shift ω is proportional to

$$I(\omega) = \int_{-\infty}^{\infty} e^{-i\omega t} \langle H'(t) H'(0) \rangle dt, \quad (7)$$

where $\langle H'(t) H'(0) \rangle$ is an appropriately defined time-dependent four-spin correlation function with the angular brackets indicating a thermal average. The time dependence of H' is governed by the spin Hamiltonian H_0 of Eq. (1),

$$H'(t) = e^{iH_0 t / \hbar} H'(0) e^{-iH_0 t / \hbar}. \quad (8)$$

Previous calculations of the overall scattering profile $I(\omega)$, which required the decoupling of time-dependent Green's functions to evaluate this correlation function, have been quite generally successful in explaining the observed scattering spectra at low temperatures. However, the extension of these techniques to higher temperatures, particularly in the region of the Néel temperature T_N and above, has met with less success. By contrast, a determination of the frequency moments of $I(\omega)$ involves the evaluation of *static* spin correlations which can often be calculated with greater reliability.

It is, of course, true that the first few moments provide one with considerably less information than is contained in the complete intensity profile so that having a theory for, say, the first moment $\langle \omega \rangle$ is in no way as satisfactory as having one for the full $I(\omega)$. Nonetheless, $\langle \omega \rangle$ is a quantity which can readily be measured experimentally and which generally can be calculated more easily than the whole spectrum. Thus it becomes possible to make meaningful comparison between theory and experiment without any adjustable parameters and normally with fewer approximations if one contents himself with the less ambitious task of analyzing the lower-order moments. Here we make comparison over the full temperature range, with particular emphasis on the paramagnetic region, $T \geq T_N$.

The integrated scattering intensity A (area), or zeroth moment, is obtained by the integration of $I(\omega)$ over all frequencies and yields the result

$$A = \langle H'(t) H'(0) \rangle_{t=0}. \quad (9)$$

Thus, the calculation of A is reduced to the evaluation of a static (time-independent) four-spin correlation. The general n th moment $\langle \omega^n \rangle$ of $I(\omega)$ can be determined from the compact expression

show later, they will permit a more meaningful comparison between theory and experiment than is

obtainable for the intensity A .

The time derivatives of H' in Eq. (10) can be readily expressed¹⁹ in terms of commutators involving H_0 and H' , and the evaluation of $\langle \omega^n \rangle$ involves static spin correlations whose complexity increases rapidly with n . For our purposes, only the first and second moments of $I(\omega)$ will be of importance and they take the forms

$$\langle \omega \rangle = \frac{1}{\hbar} \frac{\langle [H_0, H'] H' \rangle}{\langle H' H' \rangle} = \frac{1}{2\hbar} \frac{\langle [[H_0, H'], H'] \rangle}{\langle H' H' \rangle} \quad (11)$$

and

$$\langle \omega^2 \rangle = \frac{1}{\hbar^2} \frac{\langle [H_0, H']^2 \rangle}{\langle H' H' \rangle}; \quad (12)$$

we discontinue the $t=0$ notation and understand that henceforth only static spin correlations are to be considered. These moments and the intensity A include contributions from both the Stokes and anti-Stokes components of the scattered light. Since the intensity of the Stokes component, which corresponds to energy loss, is greater than that of the

anti-Stokes one, $\langle \omega \rangle$ as given by (11) is an intrinsically negative quantity. For convenience, however, we treat it as a positive quantity in specific expressions which follow so that formulas for $\langle \omega \rangle$ more properly are for $|\langle \omega \rangle|$.

The usual expression for the first moment $\langle \omega \rangle$ is given by the first equality of Eq. (11) and, due to the forms of H' and H_0 , requires the calculation of five-spin correlations in the numerator. Because of the Hermitian properties of H_0 and H' , however, $\langle \omega \rangle$ can be rewritten in the form of the second equality of Eq. (11) and the numerator is then expressible in terms of four-spin correlations, as occurs for the intensity A . Thus, the evaluations of A and $\langle \omega \rangle$ are quite similar and this will prove extremely useful in our calculations for the temperature region $T \geq T_N$. It is easily shown that all of the odd moments can be similarly rewritten. For the second moment $\langle \omega^2 \rangle$, a calculation of six-spin correlations is required.

Using the interaction Hamiltonian of Eq. (5), one obtains for the integrated scattering intensity

$$A = \langle H' H' \rangle = \frac{1}{4} \sum_{ijkl} G_{ij} G_{kl} [\langle (\vec{S}_i \cdot \vec{S}_j)(\vec{S}_k \cdot \vec{S}_l) \rangle + (\gamma - 1) \langle (\vec{S}_i \cdot \vec{S}_j) S_k^x S_l^x + S_i^x S_j^x (\vec{S}_k \cdot \vec{S}_l) \rangle + (\gamma - 1)^2 \langle S_i^x S_j^x S_k^x S_l^x \rangle]. \quad (13)$$

Here, we suppress the α, β dependence of A solely for convenience and clarification; its effects will be properly included when calculations for specific scattering geometries are undertaken. For the higher moments, we obtain the commutators

$$[H_0, H'] = i \sum_{ij} \sum_k' J_{ij} G_{jk} (\vec{S}_i \times \vec{S}_k) \cdot \vec{S}_j + i(\gamma - 1) \sum_{ij} J_{ij} \left(\sum_k' G_{jk} S_k^x (\vec{S}_j \times \vec{S}_i)^x + \frac{1}{2} G_{ij} [(\vec{S}_i \times \vec{S}_j)^x S_j^y + S_i^y (\vec{S}_j \times \vec{S}_i)^x] \right) + iD \sum_{ij} G_{ij} [S_i^x (\vec{S}_j \times \vec{S}_i)^x + (\vec{S}_j \times \vec{S}_i)^x S_j^x] \quad (14)$$

and

$$\begin{aligned} \frac{1}{2} [[H_0, H'], H'] = & -\frac{1}{2} \sum_{ij} \sum_k' J_{ij} G_{jk} \left(\sum_l'' [(G_{il} - G_{jl})(\vec{S}_i \cdot \vec{S}_k)(\vec{S}_i \cdot \vec{S}_j) + (G_{kl} - G_{il})(\vec{S}_i \cdot \vec{S}_j)(\vec{S}_i \cdot \vec{S}_k) \right. \\ & + (G_{jl} - G_{kl})(\vec{S}_i \cdot \vec{S}_i)(\vec{S}_j \cdot \vec{S}_k)] + (G_{ij} - G_{jk})(\vec{S}_j \cdot \vec{S}_k)(\vec{S}_i \cdot \vec{S}_j) + (G_{jk} - G_{ik})(\vec{S}_i \cdot \vec{S}_k)(\vec{S}_j \cdot \vec{S}_k) \\ & + (G_{ik} - G_{ij})(\vec{S}_i \cdot \vec{S}_j)(\vec{S}_i \cdot \vec{S}_k) + S(S+1)[(G_{ij} - G_{ik})(\vec{S}_j \cdot \vec{S}_k) + (G_{jk} - G_{ij})(\vec{S}_i \cdot \vec{S}_k) \\ & \left. + (G_{ik} - G_{jk})(\vec{S}_i \cdot \vec{S}_j)] \right), \quad (15) \end{aligned}$$

where the restricted sums over k and l ensure that no two spin sites are the same unless explicitly written. In Eq. (14) we include only contributions from the exchange terms J_{ij} and the anisotropy D . The effect of the dipolar term on $\langle \omega \rangle$ and $\langle \omega^2 \rangle$ is typically quite small and its general calculation is mathematically tedious. Therefore, we defer a discussion of its characteristics until such time as its inclusion is necessary for the explanation of scattering data. Likewise, in Eq. (15), we further omit the effects of the anisotropy term D and the anisotropy factor γ on the first moment $\langle \omega \rangle$. Our detailed calculations involving these parameters,

which are too complex to warrant including here, show that their effect on $\langle \omega \rangle$ is small over most of the temperature range. In particular, the anisotropy D contributes only additive terms to Eq. (15) and, thus, to $\langle \omega \rangle$.

C. Calculations for infinite and zero temperatures

The integrated intensity A is determined by a four-spin correlation function and this can be evaluated exactly in the limits of infinite temperature and of zero temperature (assuming a Néel ground state). For infinite temperature, where the spin system is totally disordered, the evaluation of this

correlation is relatively straightforward since all spin states have equal probability of being occupied. In this case, one finds

$$\langle S_i^\alpha \rangle = 0, \quad \langle S_i^\alpha S_j^\beta \rangle = \frac{1}{3} S(S+1) \delta_{ij} \delta_{\alpha\beta}. \quad (16)$$

Thus, Eq. (13) reduces to the form, for $T \rightarrow \infty$,

$$A_\infty = \frac{1}{2} \left[\frac{1}{3} S(S+1) \right]^2 (2 + \gamma^2) \sum_{ij} G_{ij}^2. \quad (17)$$

Reinserting the α, β dependence of the G_{ij} and performing the summation, Eq. (17) then becomes

$$A_\infty^{\alpha\beta} = \frac{1}{6} Z_2 N S^2 (S+1)^2 \left[\frac{1}{3} (2 + \gamma^2) \right] (G^{\alpha\beta})^2, \quad (18)$$

where N is the total number of magnetic ions in the crystal (or more appropriately, in the scattering volume) and Z_2 is the number of next-nearest neighbors, which is eight for the rutile structure. The functional dependence on the spin S is the same for the different scattering configurations, although the absolute intensity will differ because of the $G^{\alpha\beta}$ factors. Since these absolute intensities are extremely difficult to calculate and measure, we have chosen to compare the intensities (theoretical and experimental) relative to their values at zero temperature.

In principle, the calculation of the four-spin correlations at 0°K in Eq. (9) is also straightforward since only the ground state of the magnetic system is occupied. However, the true ground state for the Heisenberg system is not known and so, as a first approximation, we assume a Néel state with fully aligned spins. Within this approximation, one has the results

$$\langle S_i^\alpha \rangle = \pm S \delta_{z\alpha}, \quad \langle (S_i^x)^2 \rangle = \langle (S_i^y)^2 \rangle = \frac{1}{2} S^2, \quad (19)$$

where the + sign is to be taken for the "spin-up" sublattice, and one obtains for the zero-temperature intensity

$$A_0^{\alpha\beta} = \frac{1}{2} Z_2 N S^2 (G^{\alpha\beta})^2, \quad \alpha \neq \beta. \quad (20)$$

With the assumed Néel state, the longitudinal components $S_i^\alpha S_j^\alpha$ of H' do not contribute to $A_0^{\alpha\beta}$ for $\alpha \neq \beta$ because of the property of Eq. (6). It is also possible to compute moments for a spin-wave ground state. Details of this calculation, which is valid to all orders of magnon-magnon interactions, are presented in Appendix A. The spin-wave result increases $A_0^{\alpha\beta}$ of Eq. (20) by 9% for MnF_2 .

For the ratio of the infinite-to-zero temperature intensities, one then has

$$A_\infty/A_0 = \frac{1}{3} (S+1)^2 \left[\frac{1}{3} (2 + \gamma^2) \right], \quad (21)$$

so that, for the isotropic case ($\gamma = 1$), the integrated intensity is predicted to increase with T for $S > \frac{1}{2}$.

The ratio for MnF_2 ($S = \frac{5}{2}$) is 4.08; the spin-wave correction to the Néel state reduces this value to 3.74.

The zero-temperature $\langle \omega \rangle$ has significantly different values depending on whether a Néel or spin-wave ground state is used. For the former, Eq. (11) yields

$$\langle \omega \rangle = 2JZ/\hbar = 2\omega_{\text{ZB}}, \quad (22a)$$

for Z intersublattice neighbors coupled by an interaction J and taking $\gamma = 1$ in Eq. (5). The quantity ω_{ZB} is the frequency of a zone-boundary magnon, and thus Eq. (22a) shows that there is no decrease of $\langle \omega \rangle$ due to magnon interactions⁷ within the context of a Néel state. We regard this as a basic weakness of the Néel state for detailed zero-temperature calculations. A further difficulty is that the Néel state yields $\langle \omega^2 \rangle = \langle \omega \rangle^2$ at 0°K so that the spectrum would have zero width, which is obviously not correct since, even without interactions, the two-magnon density of states is spread over a range of spin-wave frequencies less than $2\omega_{\text{ZB}}$. It may be worthwhile to note that if the $S_i^\alpha S_j^\alpha$ terms are truncated from the interaction Hamiltonian (5) so that only two-magnon (transverse) operators are included, then the Néel state calculation gives

$$\langle \omega \rangle = 2\omega_{\text{ZB}} - J/\hbar, \quad (22b)$$

which shows just the interaction shift expected on the basis of Ising-model considerations.⁷ However, the result $\langle \omega^2 \rangle = \langle \omega \rangle^2$ also holds for the truncated Hamiltonian. Further, if anything, one might expect that removing $S_i^\alpha S_j^\alpha$ terms from H' would increase $\langle \omega \rangle$ since the longitudinal operators should contribute mainly to excitations at near-zero frequency. The results (22a) and $\langle \omega^2 \rangle = \langle \omega \rangle^2$ for $\gamma = 1$ have previously been noted.²⁰

The spin-wave calculation (Appendix A) does not suffer from the above difficulties. We find for the full H' of Eq. (5) with $\gamma = 1$,

$$\langle \omega \rangle = 2\langle \bar{\omega} \rangle - J_{\text{av}}/\hbar, \quad (22c)$$

where $2\langle \bar{\omega} \rangle$ is the value of $\langle \omega \rangle$ calculated in the absence of magnon-magnon interactions, and J_{av} is equal to J within better than 1%. Thus the spin-wave treatment, including all interaction effects, essentially reproduces the Ising-like results (22b) and is in accord with the Green's-function calculations.

Evaluation of $\langle \bar{\omega} \rangle$ for the rutile structure yields the final zero-temperature spin-wave results

$$\begin{aligned} \hbar \langle \omega \rangle^{xy} &= 16S(1 + 0.073/2S) \\ &\times [0.968J_2 - 0.126J_1 - 0.756J_3] - J_2, \end{aligned} \quad (23a)$$

$$\begin{aligned} \hbar \langle \omega \rangle^{xz} &= 16S(1 + 0.073/2S) \\ &\times [0.968J_2 - 0.378J_1 - 0.504J_3] - J_2, \end{aligned} \quad (23b)$$

in which the factor $1 + 0.073/2S$ is the Oguchi correction for energy renormalization, as discussed in Appendix A. Of particular interest is the difference

$$\hbar \langle \omega \rangle^{xz} - \langle \omega \rangle^{xy} = 16S(1 + 0.073/2S) \times (0.252)(J_3 - J_1), \quad (23c)$$

which can and will be used to extract information about the difference between the weak exchange constants J_1 and J_3 . Equations (23) neglect small dipolar corrections which will be considered later. [Note that according to Eq. (1) $J > 0$ indicates antiferromagnetic coupling so that $\langle \omega \rangle^{xz} > \langle \omega \rangle^{xy}$ for a ferromagnetic J_1 and an antiferromagnetic J_3 .]

The first moment $\langle \omega \rangle$ at infinite temperature is identically zero. The infinite-temperature second moment $\langle \omega^2 \rangle_\infty$ can be determined exactly although the calculation is somewhat lengthy. A related quantity $\langle \omega_{q_0}^2 \rangle$, the second moment at the zone boundary wave vector q_0 , has been given by Kawasaki⁹ as a function of temperature for $T \geq T_N$. For convenience, we include initially only the dominant antiferromagnetic exchange J_2 and the anisotropy factor γ , and obtain

$$\hbar^2 \langle \omega^2 \rangle_\infty^{\alpha\beta} = \frac{4}{3} Z_2 J_2^2 S(S+1) \left[1 - \frac{2}{5Z_2} \left(\frac{\gamma-1}{2+\gamma^2} \right) \times \left(1 + \frac{9}{8S(S+1)} \right) \right], \quad \alpha \neq \beta. \quad (24a)$$

For the rutile-structure antiferromagnets ($Z_2 = 8$), the anisotropy correction ($\gamma \neq 1$) will be quite small. In addition, an independent theoretical or experimental determination of γ is not currently available and we therefore neglect its effect in further calculations. If one now includes the first three neighbor exchange constants and the anisotropy D , the results are

$$\hbar^2 \langle \omega^2 \rangle_\infty^{xy} = \frac{4}{3} Z_2 J_2^2 S(S+1) \left[1 - 2 \left(\frac{Z_3}{Z_2} \right) \left(\frac{J_3}{J_2} \right) + 2 \left(\frac{Z_1}{Z_2} \right)^2 \left(\frac{J_1}{J_2} \right)^2 + 3 \left(\frac{Z_3}{Z_2} \right)^2 \left(\frac{J_3}{J_2} \right)^2 \right] + \frac{16}{15} D^2 [S(S+1) - \frac{3}{4}], \quad (24b)$$

$$\hbar^2 \langle \omega^2 \rangle_\infty^{xz} = \frac{4}{3} Z_2 J_2^2 S(S+1) \left[1 - 2 \left(\frac{Z_1}{Z_2} \right) \left(\frac{J_1}{J_2} \right) - \left(\frac{Z_3}{Z_2} \right) \left(\frac{J_3}{J_2} \right) + 6 \left(\frac{Z_1}{Z_2} \right)^2 \left(\frac{J_1}{J_2} \right)^2 + 2 \left(\frac{Z_3}{Z_2} \right)^2 \left(\frac{J_3}{J_2} \right)^2 \right] + \frac{16}{15} D^2 [S(S+1) - \frac{3}{4}], \quad (24c)$$

where we have used the tables of Rushbrooke and Wood²¹ to evaluate a number of the multispin correlations. These results show that, even in the disordered state, the weaker exchange constants,

J_1 and J_3 , yield different values of $\langle \omega^2 \rangle$ for the xy and xz (or equivalently, yz) scattering geometries. The inclusion of the dipolar terms in $\langle \omega^2 \rangle_\infty$ complicates the calculation considerably, and their contributions to the two scattering geometries are slightly different. However, it is relatively easy to show that, for the case $\gamma = 1$, there are no cross terms between the dipolar terms and either J_{ij} or D . Thus, the dipole terms only contribute additive terms to Eqs. (24a) and (24b) and lead to small relative increases in $\hbar^2 \langle \omega^2 \rangle_\infty$ on the order of $(g^2 \mu_B^2 / a_0^3)^2 / J_2^2$, where a_0 is a nnn distance.

Based on the low-temperature neutron-scattering determination^{17,18} of the exchange constants in MnF_2 , Eqs. (24b) and (24c) would predict

$$\hbar (\langle \omega^2 \rangle_\infty^{xy})^{1/2} = 23.4 \text{ cm}^{-1} \quad (24d)$$

and

$$\hbar (\langle \omega^2 \rangle_\infty^{xz})^{1/2} = 24.9 \text{ cm}^{-1}. \quad (24e)$$

For high temperatures, these values will possibly be changed due to thermal effects on the exchange constants; however, one would still expect a noticeable difference in the linewidths for the two geometries.

D. Calculations for $T \geq T_N$

Calculations of the intensity A and first moment $\langle \omega \rangle$ for other temperature ranges require knowledge of the temperature dependence of the many four-spin correlation functions incorporated into Eqs. (13) and (15); to date, reliable values for such correlations are not available. Recently, however, Ritchie and Fisher²² have obtained expressions for two-spin correlation functions based on series expansions in cubic Heisenberg ferromagnets for the paramagnetic phase ($T \geq T_C$, the Curie temperature). We now proceed to obtain appropriate expressions for A and $\langle \omega \rangle$ which will permit application of their pair correlations for the bcc lattice to the rutile-structure antiferromagnets.

1. Reduction to two-spin correlations

For the isotropic case ($\gamma = 1$), the intensity A reduces to an evaluation of correlations in the expression

$$A = \frac{1}{4} \sum_{ijkl} G_{ij} G_{kl} \langle (\vec{S}_i \cdot \vec{S}_j) (\vec{S}_k \cdot \vec{S}_l) \rangle, \quad (25)$$

where the G_{ij} are restricted to next-nearest neighbors in the rutile-structure antiferromagnets (nearest neighbors in the bcc lattice) and where repeated spin sites are allowed. Since the summations run over all possible values, the correlations to be evaluated extend over any and all sites in the full crystal. If one restricts the spin Hamiltonian H_0 to only antiferromagnetic next-nearest neighbors, then Eq. (15) becomes

$$\begin{aligned} \frac{1}{2} \langle [H_0, H'], H' \rangle = & -\frac{1}{2} \sum_{ij} \sum_k J_{ij} G_{jk} \left(\sum_l' [(G_{il} - G_{jl}) \langle \vec{S}_i \cdot \vec{S}_k \rangle \langle \vec{S}_i \cdot \vec{S}_j \rangle] \right. \\ & + (G_{kl} - G_{il}) \langle \vec{S}_i \cdot \vec{S}_j \rangle \langle \vec{S}_i \cdot \vec{S}_k \rangle + (G_{jl} - G_{kl}) \langle \vec{S}_i \cdot \vec{S}_i \rangle \langle \vec{S}_j \cdot \vec{S}_k \rangle \\ & + (G_{ij} - G_{jk}) \langle \vec{S}_j \cdot \vec{S}_k \rangle \langle \vec{S}_i \cdot \vec{S}_j \rangle \\ & \left. + G_{jk} \langle \vec{S}_i \cdot \vec{S}_k \rangle \langle \vec{S}_j \cdot \vec{S}_k \rangle - G_{ij} \langle \vec{S}_i \cdot \vec{S}_j \rangle \langle \vec{S}_i \cdot \vec{S}_k \rangle + S(S+1) [(G_{jk} - G_{ij}) \langle \vec{S}_i \cdot \vec{S}_k \rangle \right. \\ & \left. + G_{ij} \langle \vec{S}_j \cdot \vec{S}_k \rangle - G_{jk} \langle \vec{S}_i \cdot \vec{S}_j \rangle] \right). \quad (26) \end{aligned}$$

Here, no two spin sites are the same unless explicitly written. Since $J_{ij} = J_2$ and G_{jk} are restricted to nnn pairs and l is always a nnn of i , j or k , these correlations are confined to near neighbors in the lattice and the evaluation of Eq. (26) will be decidedly easier than that of Eq. (25).

The evaluation of these expressions depends on our ability to decouple the four-spin correlations into products of two-spin times two-spin correlation functions in a reliable manner. If all four indices are different, we assume the standard decoupling employed by several previous authors.²³ For our purposes we then take

$$\begin{aligned} \langle \vec{S}_i \cdot \vec{S}_j \rangle \langle \vec{S}_k \cdot \vec{S}_l \rangle = & \langle \vec{S}_i \cdot \vec{S}_j \rangle \langle \vec{S}_k \cdot \vec{S}_l \rangle \\ & + \frac{1}{3} \langle \vec{S}_i \cdot \vec{S}_k \rangle \langle \vec{S}_j \cdot \vec{S}_l \rangle + \frac{1}{3} \langle \vec{S}_i \cdot \vec{S}_l \rangle \langle \vec{S}_j \cdot \vec{S}_k \rangle \\ & (i, j, k, l \text{ unequal}) \quad (27a) \end{aligned}$$

for isotropic correlations. The case for three unequal indices $\langle \vec{S}_i \cdot \vec{S}_j \rangle \langle \vec{S}_j \cdot \vec{S}_k \rangle$ is handled by noting that such a correlation occurs in Eqs. (25) and (26) only for i and j near neighbors and j and k near neighbors (in bcc). We then find that the approximation

$$\begin{aligned} \langle \vec{S}_i \cdot \vec{S}_j \rangle \langle \vec{S}_j \cdot \vec{S}_k \rangle = & \frac{1}{3} S(S+1) \langle \vec{S}_i \cdot \vec{S}_k \rangle \\ & + \frac{2}{3} [1 - 3/4S(S+1)] \langle \vec{S}_i \cdot \vec{S}_j \rangle \langle \vec{S}_j \cdot \vec{S}_k \rangle \\ & (i \neq k) \quad (27b) \end{aligned}$$

is exact to the lowest nonvanishing order of $1/T$ in a complete high-temperature expansion and is exact to all orders in an expansion which includes only ring diagrams (high-density approximation). It is also exact for $S = \frac{1}{2}$. Similarly we take

$$\begin{aligned} \langle \vec{S}_i \cdot \vec{S}_j \rangle^2 = & \frac{1}{3} S^2(S+1)^2 - \frac{1}{2} \langle \vec{S}_i \cdot \vec{S}_j \rangle \\ & + \frac{2}{3} [1 - 3/4S(S+1)]^2 \langle \vec{S}_i \cdot \vec{S}_j \rangle^2, \quad (27c) \end{aligned}$$

which is exact under the same conditions as is (27b). The decouplings (27) appear to be the most sensible means of reducing the four-spin correlations to combinations of two-spin ones, which can then be handled in terms of the Ritchie and Fisher calculations.

With the results of (27) the integrated intensity, when normalized to the infinite-temperature result of Eq. (18), can be expressed in the form

$$\frac{A}{A_\infty} = \frac{1}{NZ_2 G^2} \sum_{ijk l} G_{ij} G_{kl} \langle \vec{S}_i \cdot \vec{S}_k \rangle$$

$$\begin{aligned} & \times \langle \vec{S}_j \cdot \vec{S}_l \rangle / S^2(S+1)^2 - \frac{3}{2S(S+1)} \langle \frac{1}{2} \frac{1}{2} \frac{1}{2} \rangle \\ & + 3 \left[\frac{1}{S(S+1)} + \frac{2}{5} \left(1 - \frac{3}{4S(S+1)} \right)^2 \right] \langle \frac{1}{2} \frac{1}{2} \frac{1}{2} \rangle^2, \quad (28) \end{aligned}$$

where there is no restriction on repeated indices in the summation. The quantity $\langle \frac{1}{2} \frac{1}{2} \frac{1}{2} \rangle$ is the pair correlation, normalized to $S(S+1)$, between a spin at the origin and one at $(\frac{1}{2}, \frac{1}{2}, \frac{1}{2})$, i. e., the correlation between nearest neighbors on opposite sublattices, and is negative for an antiferromagnet.

Since the first term in Eq. (28) is an unrestricted sum, it can conveniently be reexpressed as a sum over a single wave vector \vec{q} , so that we have

$$\begin{aligned} \frac{A}{A_\infty} = & \frac{1}{NZ_2 G^2} \sum_{\vec{q}} |G_{\vec{q}}|^2 \langle \vec{S}_{-\vec{q}} \cdot \vec{S}_{\vec{q}} \rangle^2 / S^2(S+1)^2 \\ & - \frac{3}{2S(S+1)} \langle \frac{1}{2} \frac{1}{2} \frac{1}{2} \rangle \\ & + 3 \left[\frac{1}{S(S+1)} + \frac{2}{5} \left(1 - \frac{3}{4S(S+1)} \right)^2 \right] \langle \frac{1}{2} \frac{1}{2} \frac{1}{2} \rangle^2, \quad (29) \end{aligned}$$

where

$$\langle \vec{S}_{\vec{q}} \cdot \vec{S}_{-\vec{q}} \rangle = \sum_{\vec{r}_{ij}} e^{i\vec{q} \cdot \vec{r}_{ij}} \langle \vec{S}_i \cdot \vec{S}_j \rangle \quad (30)$$

and

$$G_{\vec{q}} = \sum_{\vec{r}_{ij}} e^{i\vec{q} \cdot \vec{r}_{ij}} G_{ij}. \quad (31)$$

For the rutile-structure antiferromagnets, the $G_{\vec{q}}$ are still dependent on the particular scattering geometry studied and have the forms

$$\begin{aligned} |G_{\vec{q}}^{xy}|^2 = & Z_2^2 G^2 [\sin(\frac{1}{2}q_x a) \sin(\frac{1}{2}q_y a) \cos(\frac{1}{2}q_z c)]^2, \\ |G_{\vec{q}}^{xz}|^2 = & Z_2^2 G^2 [\sin(\frac{1}{2}q_x a) \cos(\frac{1}{2}q_y a) \sin(\frac{1}{2}q_z c)]^2, \quad (32) \end{aligned}$$

with a and c the lattice constants for the tetragonal crystal structure. Thus, the total scattering intensity, and the higher moments, will emphasize different portions of the lattice Brillouin zone for different scattering geometries. However, within the context of a single exchange constant J_2 and a bcc lattice which we used for computational purposes at $T \geq T_N$, this distinction between scattering configurations disappears.

We have also calculated the effect of a nonunity anisotropy factor γ on Eq. (29). Within the context of isotropic correlations and our decoupling scheme for the four-spin correlations, we find little change

in the results for the paramagnetic state; for reasonable values of the anisotropy γ , A/A_∞ typically shows only about a 1–2% change at T_N .

In a similar manner, we can reduce the four-spin correlations of Eq. (26) to products of two-spin correlations. If one normalizes the expression by the infinite-temperature intensity, the result is

$$\begin{aligned} & \frac{\langle [[H_0, H'], H'] \rangle}{2A_\infty} \\ &= Z_2 J_2 [2 \langle \frac{1}{2} \frac{1}{2} \frac{1}{2} \rangle - \langle 100 \rangle - \langle 110 \rangle] \\ & \times \left[1 - \frac{3}{4S(S+1)} \langle \frac{1}{2} \frac{1}{2} \frac{1}{2} \rangle - \langle 100 \rangle - \langle 110 \rangle + \langle 111 \rangle \right], \end{aligned} \quad (33)$$

where again the correlations have been normalized to $S(S+1)$. For the bcc lattice, the quantities $\langle 100 \rangle$, $\langle 110 \rangle$, and $\langle 111 \rangle$ represent pair correlations for same-sublattice near neighbors located along the cube edge, face diagonal, and body diagonal, respectively. For the antiferromagnets, all these correlations, except $\langle \frac{1}{2} \frac{1}{2} \frac{1}{2} \rangle$, are positive quantities. The first moment $\langle \omega \rangle$ is obtained by forming the ratio of Eq. (33) to Eq. (32).

Whereas the intensity expression of Eq. (32) includes correlations between all possible magnetic pairs in the crystal, the correlations of Eq. (33) are confined explicitly to magnetic ions contained in the tetragonal unit cell. This dependence of $\langle \omega \rangle$ on short-range correlations is consistent with the picture of the two-magnon line being governed by very short wavelength spin-wave-like excitations which can propagate above T_N . The dominant term in (33) is linear in the correlation $\langle \frac{1}{2} \frac{1}{2} \frac{1}{2} \rangle$ and is therefore proportional to the internal energy of the magnetic system. The magnetic specific heat, which is just the temperature derivative of the internal energy, is known to exhibit singular-type behavior in antiferromagnets at T_N and one might then expect a discontinuous thermal derivative for the numerator term of $\langle \omega \rangle$ at T_N . If the intensity varies smoothly through T_N , as the data in Sec. III would seem to indicate, then the first moment $\langle \omega \rangle$ should show indications of critical-type behavior in the region of T_N .

2. Evaluation of pair correlations

As was mentioned previously, the evaluation of the pair correlations for $T \geq T_N$, as used in (32) and (33), is based on the recent results²² of Ritchie and Fisher for two-spin static correlations in Heisenberg ferromagnets for the paramagnetic phase, $T \geq T_c$. Their study is confined to cubic lattices (sc, fcc, and bcc) of an isotropic Heisenberg system with only a single dominant exchange interaction between nearest neighbors; however, several spin values from $S = \frac{1}{2}$ to $S = \infty$ are consid-

ered. They also point out that the results are directly applicable, in magnitude, to the corresponding antiferromagnets in the classical limit, $S \rightarrow \infty$. For our purposes, their findings for the bcc lattice will be applied to the body-centered tetragonal arrangement of the rutile structure.

Based on previous work of Fisher and Burford²⁴ for the Ising system, Ritchie and Fisher²² (henceforth referred to as RF) have obtained for the Heisenberg case convenient approximants for the normalized neutron-scattering intensity function $\hat{\chi}(\vec{q}, T)$ [see Eqs. (2.16) and (6.1) of Ref. 22] at all wave vectors \vec{q} and all temperatures above the critical value T_c (for our case, we assume $T_N = T_c$). These were obtained from numerical analyses and extrapolations of high-temperature series expansions for the magnetic susceptibility, for the individual correlation functions and for the second and higher moments of the correlations. The scattering function $\hat{\chi}(\vec{q}, T)$ is just the required normalized spatial Fourier transform of the correlation function as used in Eq. (32), namely,

$$\hat{\chi}(\vec{q}, T) = \langle \vec{S}_{\vec{q}} \cdot \vec{S}_{-\vec{q}} \rangle / S(S+1). \quad (34)$$

The particular near-neighbor correlations of (32) and (33) are then obtained from the inverse Fourier transform

$$\langle \vec{S}_i \cdot \vec{S}_j \rangle = N^{-1} \sum_{\vec{q}} e^{-i\vec{q} \cdot \vec{r}_{ij}} \langle \vec{S}_{\vec{q}} \cdot \vec{S}_{-\vec{q}} \rangle. \quad (35)$$

The intensity ratio A/A_∞ and the first moment $\langle \omega \rangle$ are calculated numerically using these correlations; the required summations in \vec{q} space are carried out over 10^6 points in the full Brillouin zone. For $T \gg T_c$, the calculations are relatively accurate; however, as T approaches T_c , sizeable errors develop in the pair correlations and, therefore, in A/A_∞ and $\langle \omega \rangle$. We show in Appendix B that these errors do not result from the numerical computations but are intrinsic to the approximant $\hat{\chi}(\vec{q}, T)$, and we make simple corrections to the calculated results which serve to reduce our errors in the region of $T_c = T_N$. These corrected values for A/A_∞ and $\langle \omega \rangle$ at and near T_c are, however, to be used with caution.

Considerably more accurate values for A/A_∞ and $\langle \omega \rangle$ at $T_c = T_N$ can be obtained using the critical values for the near-neighbor correlations as given by RF. By extrapolating the high-temperature series expansions for the spatial correlations to the critical temperature, they obtain and tabulate reliable estimates for the nearest-neighbor critical correlations for the cubic lattices and several spin values; a number of the other near-neighbor correlations for the $S = \infty$ case are also listed. In addition, RF find that, for a given lattice structure, the critical spatial correlations $\langle \vec{S}_0 \cdot \vec{S}_f \rangle_c$ and $\langle \vec{S}_0 \cdot \vec{S}_f \rangle_c$ for ion pairs separated by the nearest-

neighbor distance $\vec{\delta}$ and a general distance \vec{r} , respectively, are related through the quantity [taken from Eq. (5.12) of Ref. 22]

$$D(\vec{r}) = (r/a)^{1+\eta} \langle \vec{S}_0 \cdot \vec{S}_{\vec{r}} \rangle_c / \langle \vec{S}_0 \cdot \vec{S}_{\vec{g}} \rangle_c, \quad (36)$$

which is essentially the same for a number of distinct spin models (i. e., the Heisenberg $S = \infty$ and the Ising $S = \frac{1}{2}, \infty$); here, a is the nearest-neighbor lattice spacing and $\eta \approx 0.0427$ is a critical exponent. Using Eq. (36) and the tabulated near-neighbor critical correlations for the $S = \infty$ Heisenberg system, we have obtained values for $D(\vec{r})$ and used them to extend the nearest-neighbor critical correlations for a general spin S to all \vec{r} . For $r \leq 3a$, $D(\vec{r})$ varies for each discrete \vec{r} but typically lies between 0.85 and 1.0. To estimate the critical correlations for $r > 3a$, which are not given for any S , we use the asymptotic ($\vec{r} \rightarrow \infty$) value for $D(\vec{r})$ obtained by RF using lattice Green's-function techniques; for the bcc lattice, $D(\vec{r}) \approx 0.935$. In this manner, we determine all the spatial correlations at T_c and, hopefully, are able to obtain more reliable values for A_c/A_∞ and $\langle \omega \rangle_c$ than is possible with the approximant $\hat{\chi}(\vec{q}, T)$.

In Figs. 2(a)–2(c) we plot the results of our calculations of the intensity ratio and first moment for antiferromagnets at $T \geq T_N$. Except for the $S = \frac{1}{2}$ case, we have adjusted the calculated values so that, as $T \rightarrow T_N$, the results based on the approximant $\hat{\chi}(\vec{q}, T)$ go over smoothly into the more reliable values at T_N obtained using the critical correlations. For $S = \infty$ and $S = \frac{5}{2}$ this adjustment is very small, but it does become more significant as S decreases; the difference between the two results at T_N is more pronounced for A/A_∞ than for $\langle \omega \rangle$. For the $S = \frac{1}{2}$ system, the results in the critical region are only approximate; the large discrepancy between the two correlation calculations at T_N and the general difficulty in obtaining reliable correlations for $S = \frac{1}{2}$ prevent our being more specific about the behavior near T_N .

The curves for A/A_∞ shown in Fig. 2(a) display several features of interest. For $S = \infty$, the intensity exhibits a sizeable decrease of 25% on going from high temperatures to $T = T_N$; as S decreases, the variation in intensity also decreases, showing little change for $S = 1$ and indicating an increase for $S = \frac{1}{2}$. The behavior for $S = \frac{1}{2}$ is not unexpected since Eq. (21) predicts a low- to high-temperature intensity ratio $A_0/A_\infty = 1.33$, which is increased further when the spin-wave corrections to the assumed Néel state are included. The small increases in intensity for the other low-spin values, as the temperature is reduced from $T = \infty$, is apparently real. A high-temperature series expansion of the intensity in powers of $(1/T)$ shows that, for finite S , the linear term in $(1/T)$ leads initially to an increase in intensity for antiferromagnets when T is lowered.

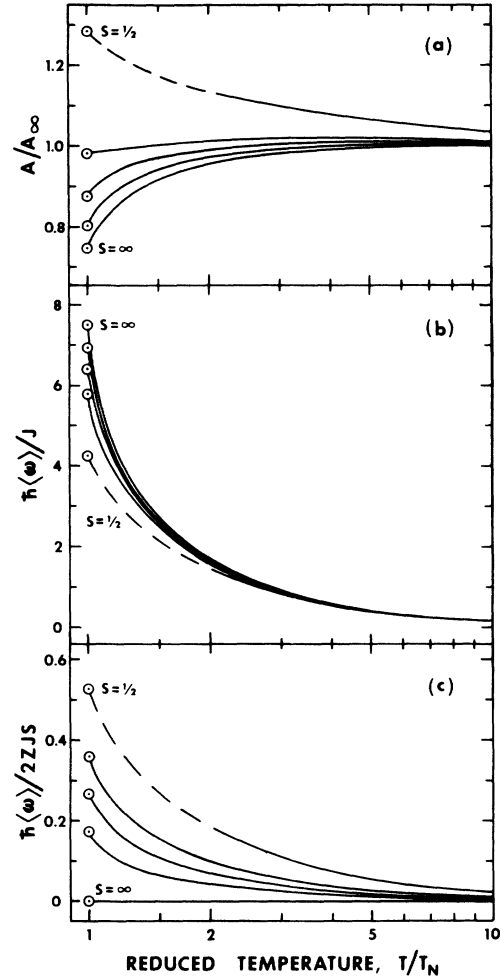


FIG. 2. Theoretical temperature dependences of the intensity and first moment for bcc antiferromagnets for $T \geq T_N$. Results for $S = \frac{1}{2}, 1, \frac{3}{2}, \frac{5}{2},$ and ∞ are presented; at fixed T , the results vary monotonically with S between the limiting curves for $S = \frac{1}{2}$ and $S = \infty$. For $S = \frac{1}{2}$, the results in the critical region are only approximate. (a) shows the integrated intensity A relative to the infinite-temperature intensity A_∞ ; (b) shows the first moment $\langle \omega \rangle$ per unit value of exchange J and (c) gives $\langle \omega \rangle$ relative to $2ZJS$, the maximum noninteracting two-magnon energy at $T = 0$.

The effect should be greatest for the smaller S but, because of the experimental error in the intensity measurement, it is probably not large enough to be observed.

The variation of the normalized first moment $\hbar(\omega)/J$, i. e., the first moment per unit value J , is given in Fig. 2(b). One notes that the curves for the various S are quite similar, except near and at T_N where the larger spin values show the larger $\langle \omega \rangle$. Generally, the first moment at T_N lies in the range $5J - 7J$. In Fig. 2(c) we plot the quantity $\hbar(\omega)/2ZJS$, where $2ZJS$ is the maximum noninter-

acting two-magnon energy at 0°K. In this case, the differences between the various S become more pronounced. For $S = \infty$, the first moment for $T \geq T_N$ is renormalized by 100% with respect to its low-temperature value. For $S = \frac{5}{2}$ the renormalization at T_N is ~85%, while it is only about 45% for $S = \frac{1}{2}$.

For completeness, we show in Figs. 3(a)–3(c) similar plots of A/A_∞ and $\langle \omega \rangle$ for the equivalent ferromagnets; for these systems all the spatial correlations are positive. The intensity variation for $S = \infty$ is the same as that for the antiferromagnet; for smaller S , the decrease in intensity is even greater as $T \rightarrow T_c$. The first moment at T_c is considerably smaller than for the antiferromagnet, with a typical value of $\hbar \langle \omega \rangle_c \approx 1.55 J$; for $S \geq 1$, $\langle \omega \rangle$ shows essentially identical behavior for all spin values over the full paramagnetic state. The decrease in intensity with a lowering of T is expected since the interaction Hamiltonian H' of Eq. (5) leads exactly to zero scattering intensity for a ferromagnet in its fully aligned ground state.

E. Calculations for $T \leq T_N$

Similar calculations of the temperature dependence of the intensity and first moment in the ordered state, $T \leq T_N$, are hampered by a lack of adequate values for the various spin-correlation functions. Recently, several authors^{11–13} have achieved limited success in predicting the temperature dependence of the two-magnon scattering peak as the Néel temperature is approached from below. Extension of their Green's-function techniques to an evaluation of the moments could be possible although the labor involved would be quite extensive. To a first approximation, however, we will utilize the simpler molecular-field theory to estimate the general behavior of A and $\langle \omega \rangle$ below $T_N(T_c)$.

In the molecular-field approximation, there are no fluctuation correlations between spins on different lattice sites so that, if the spins are chosen to order along the z direction for $T < T_N(T_c)$, one has

$$\begin{aligned} \langle S_i^x \rangle &= \langle S_i^y \rangle = 0, \\ \langle S_i^x S_j^x \rangle &= \langle S_i^y S_j^y \rangle, \\ \langle (S_i^z)^2 \rangle &= \langle (S_j^z)^2 \rangle = \frac{1}{2} [S(S+1) - \langle (S_i^z)^2 \rangle]. \end{aligned} \quad (37)$$

At $T = 0$, these results reduce to $|\langle S_i^z \rangle| \approx S$, $\langle (S_i^z)^2 \rangle \approx S^2$, and $\langle (S_i^z)^2 \rangle \approx \frac{1}{2} S$; for $T = T_N(T_c)$, one has $\langle S_i^z \rangle = 0$ and $\langle (S_i^z)^2 \rangle = \langle (S_j^z)^2 \rangle = \frac{1}{3} S(S+1)$.

Within this approximation, the intensity A^{mf} of Eq. (25) reduces to the form

$$A^{\text{mf}} = Z_2 N G^2 \left[\frac{1}{2} \langle (S_i^z)^2 \rangle - \langle (S_i^z)^2 \rangle^2 + \langle (S_i^x)^2 \rangle^2 \pm \frac{1}{4} \langle S_i^x S_j^x \rangle^2 \right], \quad (38)$$

where one uses the plus (minus) sign for the anti-ferromagnetic (ferromagnetic) system. At $T = 0$, one obtains $A_0^{\text{mf}} = \frac{1}{2} Z_2 N G^2 S^2$ for the antiferromagnets, which is the same as the result of Eq. (20); for

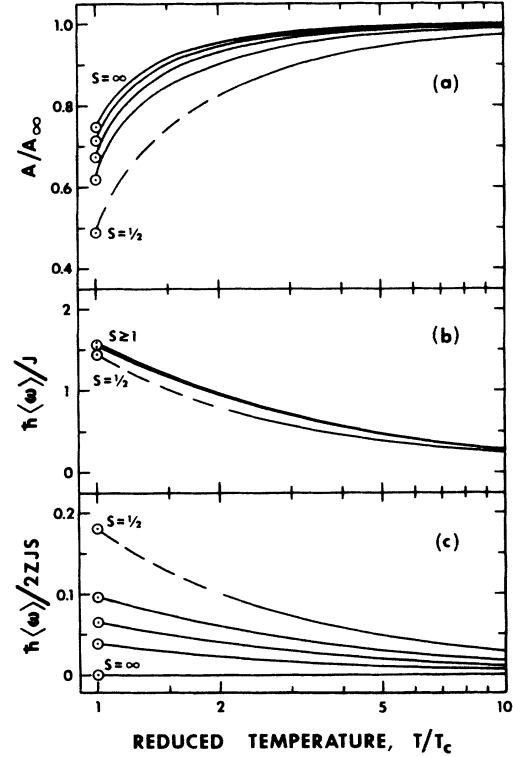


FIG. 3. Theoretical temperature dependences of the intensity and first moment for bcc ferromagnets for $T \geq T_c$. The presentation of results for $S = \frac{1}{2}$, 1, $\frac{3}{2}$, $\frac{5}{2}$, and ∞ is the same as for Fig. 2. Note that in (b) the first moment is essentially identical for all $S \geq 1$.

ferromagnets, one has $A_0^{\text{mf}} = 0$ as required by the Hamiltonian H' . By forming the ratio of Eq. (38) to A_0^{mf} , one obtains for the antiferromagnet

$$\begin{aligned} (A/A_0)^{\text{mf}} &= (1/S^2) \{ [\langle S_i^z \rangle^2 - \langle (S_i^z)^2 \rangle]^2 \\ &\quad + 2 \langle (S_i^z)^2 \rangle^2 + \frac{1}{2} \langle S_i^x S_j^x \rangle^2 \}. \end{aligned} \quad (39)$$

At $T = T_N$, $(A_c/A_0)^{\text{mf}} = \frac{1}{3} (S+1)^2$, which is the same result obtained in Eq. (21) for the ratio A_∞/A_0 . Thus, within the molecular-field approximation, the intensity varies only in the ordered state and is constant in the paramagnetic phase.

In the same manner, one obtains for Eq. (26) the result

$$\begin{aligned} \frac{1}{2} \langle [H_0, H'], H' \rangle^{\text{mf}} &= -\frac{1}{2} Z_2^2 N G^2 J_2 [S(S+1) \\ &\quad - \langle (S_i^z)^2 \rangle] [\langle S_i^z \rangle^2 \pm \langle S_i^x \rangle^2], \end{aligned} \quad (40)$$

where the signs have the same significance as previously. Here, we include only the dominant exchange J_2 in the calculation. We note that, for ferromagnets, the molecular-field theory predicts a zero first moment for *all* temperatures. For antiferromagnets, the resulting expression, when normalized to the intensity A_0^{mf} , is

$$\begin{aligned} & \left(\frac{\langle [H_0, H'], H' \rangle}{2A_0} \right)^{\text{mf}} \\ &= -\frac{2Z_2 J_2}{S^2} \langle S_i^z \rangle^2 [S(S+1) - \langle (S_i^z)^2 \rangle]. \end{aligned} \quad (41)$$

The full expression for $\langle \omega \rangle^{\text{mf}}$ is obtained by forming the ratio of Eq. (41) to Eq. (39). At $T=0$, the predicted first moment is $\hbar \langle \omega \rangle_0^{\text{mf}} = -2Z_2 J_2 S$, which is just the two-magnon energy in the absence of magnon-magnon interactions [Eq. (22a)]. For $T \geq T_N$, $\langle \omega \rangle^{\text{mf}} = 0$.

Using molecular-field theory one can calculate the predicted temperature dependences of the quantities $\langle S_i^z \rangle$ and $\langle (S_i^z)^2 \rangle$. For simplicity, however, we choose $\langle (S_i^z)^2 \rangle$ to have the form

$$\langle (S_i^z)^2 \rangle = \frac{1}{3} S(S+1) + \frac{2}{3} \langle S_i^z \rangle^2 (1 - 1/2S), \quad (42)$$

which reduces to S^2 at $T=0$ and to $\frac{1}{3} S(S+1)$ at T_N , and is independent of temperature for $S = \frac{1}{2}$ as it should be. One then obtains the results, for antiferromagnets,

$$\begin{aligned} \left(\frac{A}{A_0} \right)^{\text{mf}} &= \frac{S^2}{9} \left\{ \left(\frac{S+1}{S} \right)^2 \left[\left(\frac{M}{M_0} \right)^2 - 1 \right]^2 \right. \\ &+ 2 \left[\left(\frac{S+1}{S} \right) - \left(\frac{M}{M_0} \right)^2 \left(1 - \frac{1}{2S} \right) \right]^2 \\ &+ \left. \frac{9}{2S^2} \left(\frac{M}{M_0} \right)^2 \right\}, \quad (43) \\ \left(\frac{\langle \omega \rangle}{\langle \omega \rangle_0} \right)^{\text{mf}} &= \frac{2}{3} S \left[\left(\frac{S+1}{S} \right) - \left(\frac{M}{M_0} \right)^2 \right. \\ &\times \left. \left(1 - \frac{1}{2S} \right) \right] \left(\frac{M}{M_0} \right)^2 / \left(\frac{A}{A_0} \right)^{\text{mf}}, \end{aligned}$$

where we have replaced the ratio $\langle S_i^z \rangle / S$ with the term M/M_0 , the relative sublattice magnetization. For our purposes, the values for M/M_0 in MnF_2 will be taken directly from the published experimental results^{25,26} rather than from the molecular-field (mf) calculations.

At low temperatures, $T \ll T_N$, where the mf formalism is generally applicable, these expressions should describe the temperature dependences fairly accurately (neglecting, of course, spin-wave effects at very low temperatures). As $T \rightarrow T_N$, however, their error increases substantially. Although the molecular-field theory attempts to include properly the contributions from long-range order and same-site spin correlations, it totally neglects the effect of short-range correlations which become increasingly more important as one approaches T_N . This is evidenced by the fact that the molecular-field results show constant ($T \rightarrow \infty$) values for A and $\langle \omega \rangle$ in the paramagnetic phase. Our earlier calculations for $T \geq T_N$ show, however, that they still display appreciable temperature dependences in this region, particularly near T_N .

Since the contributions of the short-range corre-

lations below T_N are difficult to predict, we have used the following scheme to estimate more accurately A and $\langle \omega \rangle$ in the ordered state, and particularly in the critical region:

$$\begin{aligned} A &= A^{\text{mf}} + a(|T - T_N|), \\ \langle \omega \rangle &= \langle \omega \rangle^{\text{mf}} + f(|T - T_N|), \end{aligned} \quad (44)$$

where $a(|T - T_N|)$ and $f(|T - T_N|)$ are the contributions of the short-range fluctuations which are assumed to be the same for a given temperature difference above and below T_N . These terms are obtained directly from the experimental and/or theoretical results for A and $\langle \omega \rangle$ in the paramagnetic state, $T > T_N$, where long-range order is absent. For $S \geq 1$, the term $a(|T - T_N|)$ is subtractive since the A^{mf} result predicts too much intensity for $T \geq T_N$; $f(|T - T_N|)$ contributes an additive term to $\langle \omega \rangle^{\text{mf}}$. Our assumption of the forms for $a(|T - T_N|)$ and $f(|T - T_N|)$, at least in the critical region, is consistent with the results of scaling hypotheses.²⁷ We shall consider the characteristics of these approximations further in Sec. III when we discuss the experimental results.

III. EXPERIMENTAL RESULTS AND DISCUSSION

The magnetic scattering spectra of antiferromagnetic MnF_2 , NiF_2 , and RbMnF_3 were obtained using a conventional Raman-scattering facility which included an argon-ion laser, a double-grating spectrometer, a cooled phototube, and photon-counting detection. The usual 90° scattering configuration was employed with a typical instrumental resolution of 5 cm^{-1} ; on occasion, the resolution was increased to 1 cm^{-1} to study the scattering characteristics close to the laser excitation frequency. Temperature control was achieved with a variable-temperature Dewar which used a flowing He exchange gas, except at 2°K where the sample was immersed in superfluid He. A given temperature could be stabilized to better than 0.1°K over long times, although we estimate our value for the temperature in the scattering volume to be accurate only to $\pm 5, -3^\circ \text{K}$.

The oriented single crystals were fabricated from high-optical-quality material which showed very little parasitic scattering. The majority of the magnetic scattering spectra were obtained in the $x(yx)y$ scattering configuration, with the incident and scattered light polarizations normal to each other and to the crystal c axis. Spectra for the $x(yz)y$ geometry in MnF_2 , wherein the polarization of one of the light waves lies along the c axis, showed essentially the same behavior although the intensity was about a factor of 2 less. In addition, the scattering of the E_g phonon line ($\sim 245 \text{ cm}^{-1}$) was also measured in MnF_2 . By comparing the observed temperature dependence of the

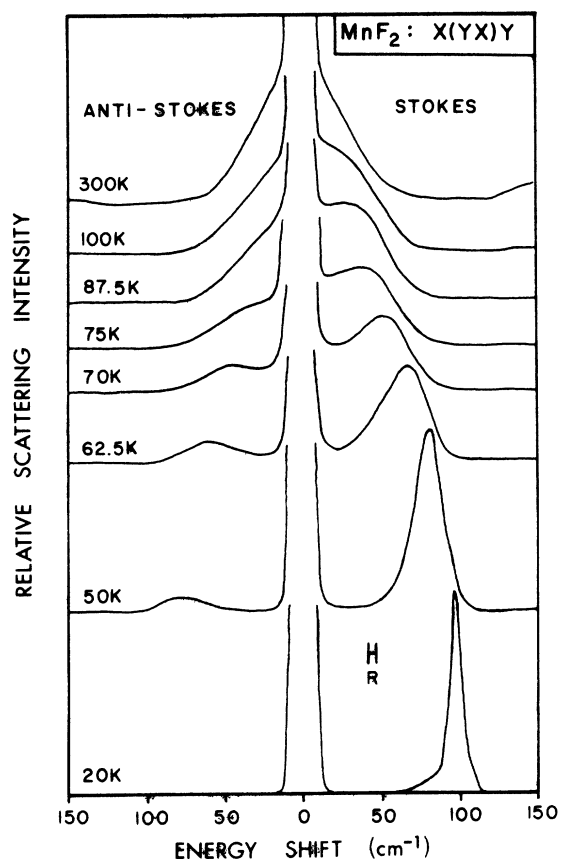


FIG. 4. Typical magnetic light scattering spectra in antiferromagnetic and paramagnetic MnF_2 ($T_N = 67.7^\circ\text{K}$). The instrumental resolution of 5 cm^{-1} is denoted by the vertical bars.

integrated scattering intensity for the E_g phonon to its predicted behavior, one can determine the effect of varying experimental conditions and of any temperature-dependent absorption characteristics in MnF_2 on the scattering profiles, and the magnetic scattering spectra is then suitably corrected for such effects. Furthermore, all data were obtained using the $4579\text{-}\text{\AA}$ laser excitation to minimize laser light absorption and to eliminate sample fluorescence in the region of the magnetic scattering spectra.

In Fig. 4 we show typical magnetic scattering spectra for MnF_2 as obtained in the $x(yx)y$ geometry. At low temperatures the spectrum is characterized by the usual two-magnon line at $\sim 100 \text{ cm}^{-1}$ as has been previously reported.² As the temperature is raised, the scattering increases in intensity and the scattering peak moves to lower frequency shifts until, at temperatures well above the Néel temperature $T_N = 67.7^\circ\text{K}$, the spectrum is characterized by a symmetric near-Gaussian line centered at zero frequency shift. Note, in particu-

lar, that on going from 70 to 62.5°K there is a marked decrease in scattering intensity near zero frequency shift, whereas the scattering peak shows relatively little change in position. Such behavior indicates that the first moment $\langle\omega\rangle$ is changing much more rapidly than the two-magnon frequency in the critical region.

The temperature dependence of the integrated scattering intensity (both Stokes and anti-Stokes components) relative to its 2°K value is shown in Fig. 5; the intensity has been corrected for experimental and absorption effects as discussed previously. Data for the $x(yx)y$ and $x(yz)y$ scattering geometries show essentially identical behavior. The observed increase in intensity with increasing temperature is in qualitative agreement with theory, but contrary to the earlier reported results³ of a decrease in intensity for the isomorphous NiF_2 system. (More recent work¹⁶ in NiF_2 shows that the scattering intensity does increase if the raw data are properly corrected for a strongly temperature-dependent optical absorption effect.) As seen in Fig. 5, the observed high-temperature intensity for MnF_2 exceeds its 2°K value by a factor of 4.45 which is significantly larger than the predicted ratio, $A_\infty/A_0 \approx 3.74$. The predicted intensity variation for $T \geq T_N$, which is based on the evaluation of the static correlations of Eq. (32), is also given in Fig. 5. One notes that the predicted 25% increase in intensity from T_N to infinite temperature

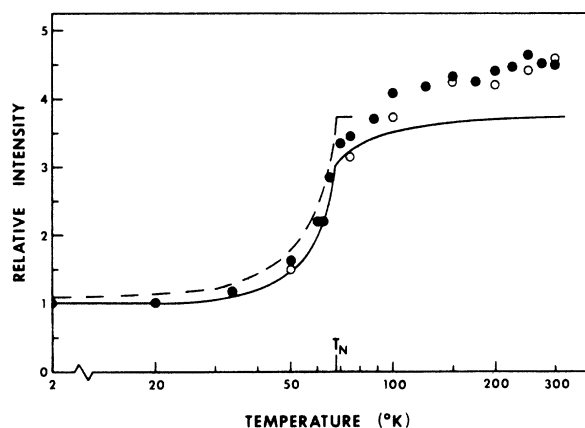


FIG. 5. Temperature dependence of the magnetic scattering intensity in MnF_2 . The solid and open circles give the observed integrated scattering intensity relative to its 2°K value for the $x(yx)y$ and $x(yz)y$ scattering geometries, respectively. Above T_N , the solid curve shows the theoretical relative intensity based on the results of Fig. 2(a). For $T \leq T_N$, the dashed curve is the predicted intensity A^{mf} based on molecular-field theory whereas the solid curve is the intensity obtained by combining A^{mf} and the theoretical results for $T \geq T_N$, as discussed in the text.

is only about half as large as is observed.²⁸

An anisotropy $(\gamma - 1) \approx 0.25$ is one possible means to remove the observed discrepancy in A_∞/A_0 , although such a large value does seem unlikely. Besides, as our discussion of Eq. (32) pointed out, a nonunity γ of this magnitude in MnF_2 will have negligible effect on the predicted intensity variation for $T \geq T_N$ and, therefore, cannot reproduce the data for the paramagnetic regime. We have further considered the possibility that a strongly temperature-dependent scattering at zero frequency shift due to extraneous mechanisms, such as second-order phonon scattering, etc., might occur and could lead to an apparent increase in magnetic scattering intensity at high temperatures. A comparison of the scattering intensities near zero frequency shift at 300°K for the $z(xx)y$ scattering geometry, where the magnetic intensity is small and where two-phonon scattering is expected to be large, and for the $z(yx)y$ configuration would indicate, however, that this effect is unimportant.

The increases at high T could also result from thermal effects on the ground-state-excited-state exchange parameters, on the many scattering cross-section parameters, and on the assumed constant relationship between the phonon and magnetic scattering, as used in the intensity correction process; unfortunately, the effects of these processes on the spectra are difficult to assess. We do note, however, that the measured intensity ratio of ~ 3 at T_N agrees extremely well with the predicted value of $A_c/A_0 \approx 3.0$, which is obtained by extending our theoretical intensity curve down from the predicted high-temperature ratio, $A_\infty/A_0 \approx 3.74$.

A similar discrepancy²⁹ between the theoretical and experimental intensity variation in the paramagnetic state has also been observed¹⁶ in the NiF_2 system. The measured high-temperature-intensity ratio exceeds the predicted value by about 20%, whereas the predicted intensity variation between T_N and infinite temperature is only about 2%. Here also, however, one obtains good agreement between experiment and theory for the intensity ratio at T_N .

In the ordered state we use the molecular-field results of Eq. (44) to estimate the behavior of the scattering intensity. The dashed curve of Fig. 5 represents the contribution of the A^{mf} of Eq. (44) as obtained from published values^{25,26} for the relative sublattice magnetization in MnF_2 ; this curve has been normalized to account for the spin-wave corrections to the intensity at very low temperatures. The solid curve represents the full estimate for A when the short-range fluctuation term $a(|T - T_N|)$ is included in the calculation. Here, we use the *theoretical* A for $T > T_N$ to obtain directly the form of $a(|T - T_N|)$ rather than the experimental values, because of the anomalous increase

in the latter for $T > T_N$. The resultant A is seen to give reasonable agreement with the data in the critical region. More accurate calculations for the ordered phase, based possibly on the spin-wave techniques¹¹⁻¹³ mentioned in Sec. II E, may improve the agreement between experiment and theory.

The exact reason for the increased scattering intensity in the paramagnetic phase for MnF_2 , and for the isomorphous NiF_2 system, is not known. The good agreement between the experimental and theoretical values for A_c/A_0 would appear to indicate, however, that the problem occurs only at high temperatures and that the observed temperature variation of the intensity in the ordered phase is behaving properly, even though reliable calculations for this region are not currently available. Further studies in other systems would be of use in determining if this behavior at high T is a general feature of the magnetic scattering in antiferromagnets. Measurements in cubic antiferromagnets, where $\gamma = 1$, would be particularly useful in this regard; unfortunately, such intensity measurements in cubic systems are extremely difficult since there are typically no first-order phonon lines in most of those materials to aid in correcting for absorption, etc.

In Fig. 6 we show the observed temperature dependences of the first moment $\langle \omega \rangle$ of the integrated scattering intensity and the energy shift of the Stokes scattering peak. The smooth variation in the scattering peak energy over the temperature range, even through T_N , is quite similar to previously reported behavior in NiF_2 and several other antiferromagnets^{3,4}; at T_N , the two-magnon energy (as inferred from the peak position) is renormalized by about 45%. By contrast, the first moment shows a much more pronounced decrease with increasing temperature and, at T_N , is reduced to 15% of its low-temperature value. Also, the data near T_N appear to indicate a discontinuity in the temperature derivative of $\langle \omega \rangle$ at T_N , as compared to the apparently smooth behavior of the scattering peak frequency and the intensity in this same region. Such behavior is not unexpected, as our previous calculations would indicate that $\langle \omega \rangle$ should show critical-type behavior near T_N . This behavior could prove useful as a means for studying the near-neighbor correlations in the critical region.

Since the first moment is normalized relative to the total scattering intensity, a more meaningful comparison between experiment and theory is expected for $\langle \omega \rangle$ than was obtained for the intensity. The solid curve for $T \geq T_N$ in Fig. 6 is the predicted temperature dependence for $\langle \omega \rangle$ based on expressions (32) and (33) and on the pair correlations of Ritchie and Fisher. The results contain no adjustable parameters since the value of the dominant nnn exchange constant J_2 is taken directly from the

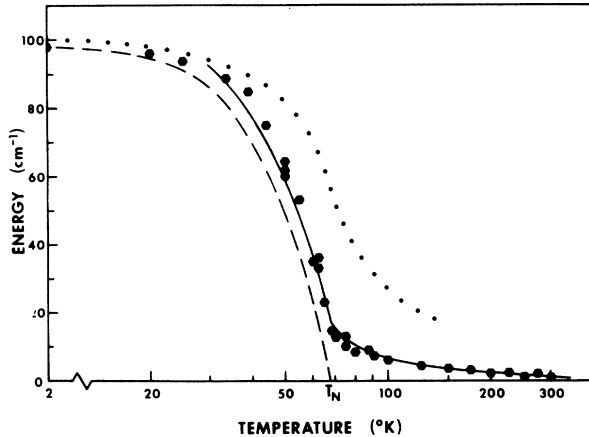


FIG. 6. Temperature dependence of several aspects of magnetic scattering in MnF_2 . The hexagons are the observed first moment $\langle\omega\rangle$ for the total magnetic scattering in the $x(yx)y$ configuration. Above T_N , the solid curve is the predicted $\langle\omega\rangle$ obtained from the results of Figs. 2(b) and 2(c). For $T \leq T_N$, the dashed curve is the predicted $\langle\omega\rangle^{mf}$ based on molecular-field theory and the solid curve is the full $\langle\omega\rangle$ obtained by combining $\langle\omega\rangle^{mf}$ with the $\langle\omega\rangle$ for $T \geq T_N$, as discussed in the text. The dotted curve is the observed energy shift for the Stokes scattering peak in the $x(yx)y$ scattering geometry.

neutron scattering data^{17,18} for MnF_2 . The agreement between theory and experiment is quite good over the full range and particularly at T_N , where the predicted value of 17 cm^{-1} is to be compared with the observed $\langle\omega\rangle = 15 \text{ cm}^{-1}$. The inclusion of the nn exchange J_1 , which is really not negligible for MnF_2 , into the theory might improve the agreement at T_N ; however, calculations of the spin correlations for a Heisenberg system with several exchange constants are not presently available.

In the ordered phase we again use the molecular-field approximation to estimate the temperature dependence of $\langle\omega\rangle$. The dashed curve of Fig. 6 is the $\langle\omega\rangle^{mf}$ of Eq. (44) based on the published sublattice magnetization results,^{25,26} whereas the solid curve includes the short-range fluctuation contribution $f(|T - T_N|)$. In this case, $f(|T - T_N|)$ is taken from the combined theoretical and experimental behavior of $\langle\omega\rangle$ in the paramagnetic phase. Again, we obtain reasonable agreement with experiment in the critical region, although more accurate calculations for the ordered phase are still required.

The spectra at 2°K have been analyzed for the first moment and the resulting $\langle\omega\rangle$ compared with Eqs. (23) for MnF_2 and NiF_2 . The corresponding equation for cubic RbMnF_3 is

$$\hbar\langle\omega\rangle = 12S(1 + 0.097/2S)(0.946J) - J, \quad (45)$$

independent of scattering geometry, assuming a single nearest-neighbor ($Z = 6$) exchange constant.

Table I shows the measured first moments and those calculated from Eqs. (23) and (45) using published neutron-scattering measurements of the exchange constants.^{18,30,31} We have put in dipolar corrections to $\langle\omega\rangle^{\alpha\beta}$ which are of the order of 1 cm^{-1} or less for noncubic MnF_2 and NiF_2 . These have been calculated using the Néel ground state for simplicity. A single-ion anisotropy interaction DS_1^2 is also important in NiF_2 , and its contribution of $(2S - 1)D$ to $\langle\omega\rangle^{\alpha\beta}$ has been included. Agreement between experiment and theory, together with the published exchange constants, is seen to be quite good.

The difference $\langle\omega\rangle^{xz} - \langle\omega\rangle^{xy}$ can be used to infer a light scattering value for $J_3 - J_1$ according to Eq. (23c). The so-determined numbers for $J_3 - J_1$ are shown in Table II together with the neutron results. Agreement is quite good for MnF_2 but less satisfactory for NiF_2 , although within experimental error. We feel that our value $J_1 \approx J_3$ for NiF_2 is the more accurate, both because of the larger quoted errors on the neutron measurements and because a $J_3 - J_1$ as large as 1 cm^{-1} predicts a 4-cm^{-1} difference between $\langle\omega\rangle^{xz}$ and $\langle\omega\rangle^{xy}$ which would be easily detected in our experiment, whereas the xz and xy moments are nearly identical.

In Figs. 7(a) and 7(b) we show spectra for the $x(yx)y$ and $x(yz)y$ scattering configurations obtained at 300°K using an instrumental resolution of 1.5 cm^{-1} ; even with this relatively high resolution, we are unable to approach closer to the laser line than a few cm^{-1} due to the relatively strong Brillouin scattering from the acoustic phonon modes. One notes the pronounced differences in the linewidths for these two spectra. The measured values of $(\langle\omega^2\rangle^{xy})^{1/2} = 25.5 \text{ cm}^{-1}$ and $(\langle\omega^2\rangle^{yz})^{1/2} = 28.6 \text{ cm}^{-1}$ are to be compared with the predicted high-temperature results, $(\langle\omega^2\rangle_{\infty}^{xy})^{1/2} = 23.4 \text{ cm}^{-1}$ and $(\langle\omega^2\rangle_{\infty}^{yz}) = 24.9 \text{ cm}^{-1}$, given by Eqs. (24d) and (24e); for MnF_2 , the high-temperature ($T \rightarrow \infty$) limit should be fairly well satisfied at room temperature. Although our measured results are about 10% larger than the predicted values, the increased width for the yz spectrum over the xy is as expected and points up the influence of the weaker exchange constants, J_1 and J_3 , on the high-temperature spectra.

The increase in the measured $\langle\omega^2\rangle$ over the predicted results is not fully understood; it might arise from thermal effects on the exchange parameters but there is a strong possibility that much of the disagreement is experimental in origin. Because of the limited signal-to-noise ratio, it is difficult to obtain reliable data in the far wings of the spectrum, where slight increases in intensity can cause noticeable increases in the higher moments. In addition, our inability to acquire data very close to the laser line can have pronounced effects on the measured $\langle\omega^2\rangle$; presently, we estimate the be-

TABLE I. Theoretical and experimental values of $\langle \omega \rangle$ together with values of parameters used. All numbers are in cm^{-1} .

Material	Parameters used in calc.	Theory		Expt. (this work)	
		$\langle \omega \rangle^{xy}$	$\langle \omega \rangle^{xz}$	$\langle \omega \rangle^{xy}$	$\langle \omega \rangle^{xz}$
RbMnF ₃	$J = 4.72 \pm 0.42^a$	131.8 ± 12	131.8 ± 12	131.4 ± 0.5	
MnF ₂	$J_1 = -0.45 \pm 0.02^b$ $J_2 = 2.45 \pm 0.02^b$ $J_3 = 0.065 \pm 0.02^b$ dipole-dipole	95.5 ± 1.5	100.2 ± 1.5	97.6 ± 0.7	102.9 ± 0.7
NiF ₂	$J_1 = -0.21 \pm 0.50^c$ $J_2 = 13.38 \pm 0.36^c$ $J_3 = 0.76 \pm 0.40^c$ $D = 4.36 \pm 0.14^c$ dipole-dipole	196.3 ± 11	200.5 ± 11	201.1 ± 0.7	201.5 ± 0.7

^aReference 30 (J as defined here is called $2J$ in Refs. 30 and 18).

^bReference 18.

^cReference 31. The single-ion term E is not included since it does not affect $\langle \omega \rangle$. Values of J found in Ref. 31 have been reduced by 3.7% to account for the Oguchi correction.

havior of the spectrum near $\omega = 0$ based on theoretical results³² which treat the line shape of the high-temperature scattering profile in terms of a generalized diffusivity model. Finally, the presence of appreciable nonuniform background scattering, as is particularly evident in our $x(yz)y$ spectrum of Fig. 7(b), introduces significant uncertainty into the measured $\langle \omega^2 \rangle$. Further more comprehensive studies of these high-temperature spectra are planned to see if one can obtain reliable values for $\langle \omega^2 \rangle$ with meaningful error limits on the results. Such measurements could then prove useful for studies of the temperature and pressure dependences of the exchange parameters in the paramagnetic phase.

IV. SUMMARY AND CONCLUSIONS

We have calculated the low-order frequency moments for two-spin fluctuation light scattering in the rutile-structure antiferromagnets as a function of temperature and have compared the results with comprehensive measurements in the MnF₂ system. The moments (including intensity, the zeroth moment) are directly related to static spin-correlation functions, which can generally be computed with reasonable reliability, and do not require the same decoupling procedures of dynamical equations as are needed to calculate the overall spectral line shape. The determination of the moments provides another test for the general theories of light scattering in magnetic systems and, in particular, permits the first direct comparison between theory and experiment for the paramagnetic state.

Expressions for the scattering intensity A and first moment $\langle \omega \rangle$ for all temperatures from well below to well above the Néel temperature T_N are obtained. They are evaluated exactly in the limits

of infinite temperature and of zero temperature within the spin-wave formalism. For the inter-

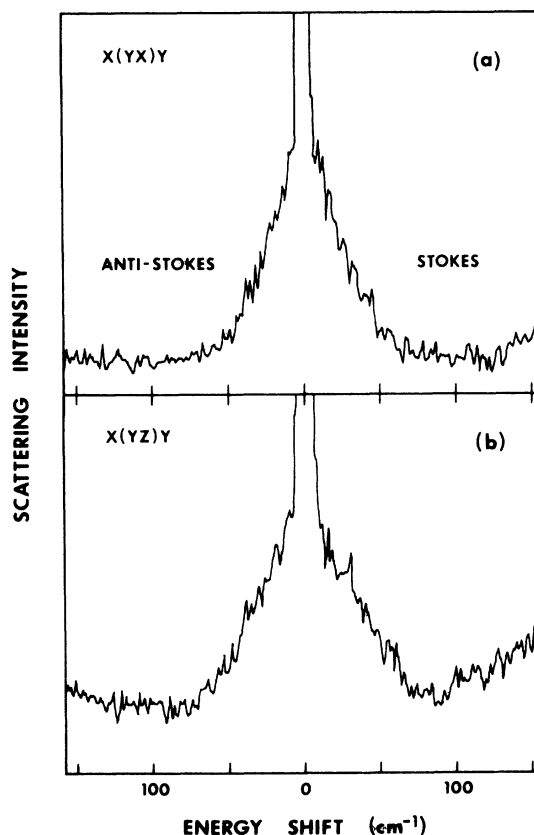


FIG. 7. Spectra of magnetic light scattering in paramagnetic MnF₂ at 300°K. Instrumental resolution is 1.5 cm^{-1} . (a) and (b) are spectra obtained in the $x(yx)y$ and $x(yz)y$ scattering configurations, respectively.

TABLE II. Properties of weak exchange constants J_1 and J_3 .

Material	$J_3 - J_1$, this work ^a	$J_3 - J_1$, neutron data
MnF ₂	$0.59 \pm 0.14 \text{ cm}^{-1}$	$0.52 \pm 0.04 \text{ cm}^{-1}$ ^b
NiF ₂	$0.07 \pm 0.35 \text{ cm}^{-1}$	$1.0 \pm 0.90 \text{ cm}^{-1}$ ^c

^aInferred from observed $\langle \omega \rangle_{xx} - \langle \omega \rangle_{xy}$ and Eq. (23c) plus dipolar corrections.

^bReference 18.

^cReference 31.

mediate temperature region, the required correlations are determined using suitable approximations. In the paramagnetic phase, $T \geq T_N$, the multispin correlations are decoupled into products of two-spin correlations which are then evaluated using previously published results of Ritchie and Fisher²² for pair correlations in Heisenberg ferromagnets. In the ordered state, $T \leq T_N$, A and $\langle \omega \rangle$ are estimated using the molecular-field formalism to describe the effects of long-range correlations and the results of the paramagnetic phase to characterize the behavior of the short-range fluctuations. In addition, we also obtain exact expressions for the second moment $\langle \omega^2 \rangle$ in the infinite-temperature limit.

In general, the measured spectral moments for MnF₂ are in good agreement with the theoretical results. The integrated scattering intensity increases with increasing temperature, showing its most pronounced variation in the region of T_N . The measured ratio of the intensity at T_N to the zero-temperature value agrees very well with theory; in the paramagnetic phase, however, we observe at high T an anomalous increase of $\sim 20\%$ in the intensity over its predicted behavior, which remains unexplained.

The first moment $\langle \omega \rangle$, on the other hand, decreases with increasing temperature and shows quite good agreement with theory, which contains no adjustable parameters, over the full temperature range. In the paramagnetic phase, in particular, the agreement is very good, even near and at T_N . The measured $\langle \omega \rangle$ shows pronounced rapid changes in the region near T_N ; by contrast, the peak of the scattering spectrum, which has been of primary interest in previous studies, shows a smooth variation with changing temperature, even through T_N . These changes in $\langle \omega \rangle$ show indication of critical-type behavior near T_N and could prove useful for studies of the dynamics of short-range correlations in the critical region.

The fact that we do obtain good absolute agreement above T_N for $\langle \omega \rangle$, which is insensitive to thermal effects on the scattering parameters,

makes us believe that the methods and correlation functions we have used are basically correct. It thus seems more likely that the anomalous behavior in the total intensity above T_N is due to some extraneous temperature dependence of the parameters which cancels in the numerator and denominator of the expression for $\langle \omega \rangle$ than due to some fundamental inadequacy of the calculation of $\langle H'H' \rangle$ for the model system.

Detailed comparison between theory and experiment has been made for $\langle \omega \rangle$ in the zero temperature limit for RbMnF₃ and NiF₂, as well as for MnF₂. Good agreement is found. Of particular interest here is the fact the difference $\langle \omega \rangle_{xx} - \langle \omega \rangle_{xy}$ can be used to infer the difference $J_3 - J_1$ between the weak exchange constants in rutile-structure antiferromagnets. It appears likely that at least for NiF₂ light scattering provides a more reliable value for $J_3 - J_1$ than does neutron scattering. This is an illustration that analysis of the spectra by moments can provide a quick answer for certain of the more subtle properties of the exchange constants. It is, however, possible to get the same and possibly more information about J_1 and J_3 from fitting³³ low-temperature intensity profiles to Green's-function calculations, but the computational procedures involved are likely to be much more tedious.

At high temperatures, the spectrum is characterized by a symmetric line centered at zero frequency shift; an analysis of the overall spectral profile is given elsewhere.³² The variation in the second moment $\langle \omega^2 \rangle$ for different scattering geometries, which results from the presence of several exchange constants, is in qualitative agreement with our infinite-temperature calculations, although the measured $\langle \omega^2 \rangle$ are about 20% larger than predicted. Much of the discrepancy is believed due to experimental effects and further studies of these high-temperature spectra are planned. If the experimental difficulties can be resolved, however, the measured $\langle \omega^2 \rangle$ could provide an effective and convenient technique for determining the temperature and pressure dependences of the exchange parameters in the paramagnetic phase.

ACKNOWLEDGMENT

The authors are especially indebted to R. R. Bartkowski, whose initial thoughts and calculations form a basis for portions of this work.

APPENDIX A: SPIN-WAVE EVALUATION OF $\langle \omega \rangle$

We start with the Dyson-Maleev description of spin operators:

$$S_i^x = S - a_i^\dagger a_i, \quad (\text{A1a})$$

$$S_j^y = -S + b_j^\dagger b_j, \quad (\text{A1b})$$

$$S_i^z = (2S)^{1/2} a_i, \quad (\text{A1c})$$

$$S_i^+ = (2S)^{1/2} a_i^\dagger (1 - a_i^\dagger a_i / 2S), \quad (\text{A1d})$$

$$S_j^+ = (2S)^{1/2} b_j, \quad (\text{A1e})$$

$$S_j^- = (2S)^{1/2} (1 - b_j^\dagger b_j / 2S) b_j, \quad (\text{A1f})$$

where a_i and b_j are Boson spin-deviation annihilation operators for the "up" and "down" sublattices, respectively. Diagonalization of the quadratic part of H_0 yields a set of noninteracting magnons whose Boson annihilation operators α_k and β_k are related to a_k and b_k ($a_k = N^{-1/2} \sum_i a_i e^{i\mathbf{k} \cdot \mathbf{r}_i}$, etc.) by

$$a_k = \lambda_k \alpha_k + \mu_k \beta_k^\dagger \quad (\text{A2a})$$

and

$$b_k = \lambda_k \beta_k + \mu_k \alpha_{-k}^\dagger, \quad (\text{A2b})$$

where λ_k and μ_k are coefficients of the Holstein-Primakoff or Bogoliubov transformation. (The above relations, in which the transformation involves only two parameters and the modes are degenerate in the absence of an applied field, assumes uniaxial anisotropy with respect to the equilibrium z direction.)

Use of (A1) and (A2) in (1) and (5) then produces an H_0 and an H' which contain combinations of four-magnon operators as well as quadratic terms. Evaluation of $\langle \omega \rangle$ then in principle involves handling a multitude of expressions each of which can contain as many as ten magnon operators $\{im [H_0^{(4)}, H'^{(4)}] H'^{(4)}, \text{ten-magnon terms result since } [H_0^{(4)}, H'^{(4)}] \text{ has six-magnon terms, where the superscript (4) indicates four-magnon parts}\}$, and the task would likely be impossible for a person with average patience and life span if it were not for simplifications at 0°K which are discussed below.

The major simplification is that we are only interested in that part of H' which describes the net excitation of two magnons, since other parts of H' will contribute to the intensity at points ($\omega = 0$ and $\omega = 4\omega_{\text{ZB}}$) far removed from the main two-magnon line. This amounts to truncating the Hamiltonian in a manner similar to that in calculating moments of the magnetic resonance line.³⁴

The renormalization of H' into an effective two-magnon excitation Hamiltonian has been treated in some detail by Davies.³⁵ His result may be written [we henceforth take $\gamma = 1$ in Eq. (5)]

$$\begin{aligned} H'(\text{two-magnon}) &= \frac{1}{2} \sum_{ij} G_{ij}^{\alpha\beta} \vec{S}_i \cdot \vec{S}_j(\text{two-magnon}) \\ &= \sum_k g_k \alpha_k^\dagger \beta_{-k}^\dagger + \text{H. c.}, \end{aligned} \quad (\text{A3})$$

at zero temperature, where it is exact within the spin-wave formalism, in which

$$g_k = G_k^{\alpha\beta} S (\lambda_k^2 + \mu_k^2) (1 + c), \quad (\text{A4})$$

$G_k^{\alpha\beta}$ is the Fourier transform of $G_{ij}^{\alpha\beta}$, and c is the Oguchi correction³⁶ to the spin-wave energy. The

above expression for g_k assumes that $G_{ij}^{\alpha\beta}$ and J_{ij} are confined to nearest intersublattice neighbors. The interaction corrections to g_k , represented by c , are wave-vector independent. Part of the contribution to c comes from the four-magnon part of $S_i^+ S_j^-$; so the longitudinal part of $\vec{S}_i \cdot \vec{S}_j$ does affect the two-magnon line, contrary to the Néel state result for $\langle H'H' \rangle$. The integrated intensity is given immediately by

$$\langle H'H' \rangle = \sum_k g_k^2. \quad (\text{A5})$$

Numerical values of (A5) relative to the Néel result are presented in Table III.

The first-moment numerator $\langle [H_0, H'] H' \rangle$ may now be considered. The Hamiltonian H_0 contains many four-magnon terms, but only a limited number can contribute to $\langle \omega \rangle$ at $T=0$, and their character can readily be identified. We first express H_0 in the form

$$H_0 = \sum_k \hbar \tilde{\omega}_k (\alpha_k^\dagger \alpha_k + \beta_k^\dagger \beta_k) + H_0^{(4)} = H_0^{(2)} + H_0^{(4)}, \quad (\text{A6})$$

where $H_0^{(4)}$ is a "true" four-magnon Hamiltonian in which all creation operators stand to the left, and $\tilde{\omega}_k$ includes all renormalizations which occur in the process of moving creation operators to the left in the formation of $H_0^{(4)}$. That is, a four-spin deviation term such as $\alpha_k \alpha_k^\dagger \beta_{k'}^\dagger \beta_{k'}$ is rewritten

$$\alpha_k \alpha_k^\dagger \beta_{k'}^\dagger \beta_{k'} = \alpha_k^\dagger \alpha_k + \alpha_k^\dagger \beta_{k'}^\dagger \alpha_k \beta_{k'}, \quad (\text{A7})$$

upon making use of the Boson commutation relations. The first term in (A7) becomes part of a new quadratic Hamiltonian $H_0^{(2)}$ which contains the corrected spin-wave energy $\tilde{\omega}_k$ as treated by Oguchi,³⁶ and the remaining term in (A7) becomes part of $H_0^{(4)}$ in Eq. (A6).

The contribution of the quadratic part of (A6) to the first-moment numerator is readily calculated to be

$$\langle [H_0^{(2)}, H'] H' \rangle = -2\hbar \sum_k \tilde{\omega}_k g_k^2. \quad (\text{A8})$$

TABLE III. Ratio of integrated intensities in spin-wave ground state to that in Néel state, A (spin wave)/ A (Néel state), assuming one dominant exchange constant. The coefficient involving S is $(1+c)^2$, where c is the Oguchi correction.

Lattice type	A (spin wave) A (Néel state)	Value for particular compound
Simple cubic	$(1.101)(1 + 0.097/2S)^2$	1.144, RbMnF ₃
Rutile (or bcc)	$(1.061)(1 + 0.073/2S)^2$	1.140, NiF ₂ 1.092, MnF ₂

A more lengthy calculation gives, at zero temperature,

$$\langle [H_0^{(4)}, H'] H' \rangle = N \sum_j J_{ij}^{(0)} g_{ij}^2, \quad (\text{A9})$$

in which g_{ij} is the spatial Fourier transform of g_k , N is the number of spins on a sublattice, and the superscript (0) on J_{ij} indicates opposite sublattice couplings only. [Dipolar and single-ion anisotropy contributions to (A9) are negligible and have been left out.] An interesting feature is that the only part of $H_0^{(4)}$ which contributes to (A9) comes from the four-spin deviation operators in the longitudinal $S_i^z S_j^z$ terms of H_0 with i and j on opposite sublattices. Contributions from the transverse terms all cancel to give zero.

By using Eqs. (A5), (A8), and (A9) in (11) we then have

$$\langle \omega \rangle = 2 \langle \tilde{\omega}_k \rangle - J_{av}^{(0)} / \hbar, \quad (\text{A10})$$

where $\langle \tilde{\omega}_k \rangle$ is the average magnon energy weighted with respect to the interaction g_k^2 and where

$$J_{av}^{(0)} = \sum_j J_{ij}^{(0)} g_{ij}^2 / \sum_j g_{ij}^2 \quad (\text{A11})$$

is the average intersublattice coupling weighted with respect to g_{ij}^2 . The quantities g_k and $G_k^{\alpha\beta}$ are related by Eq. (A4), and we note that since the multiplicative correction to g_k , $(1+c)$, is wave-vector independent, it cancels out of the expressions. Thus the quantity $2 \langle \tilde{\omega}_k \rangle$ in (25) represents the first moment which would be calculated for a completely noninteracting set of magnons (but whose frequencies do contain the Oguchi corrections).

Since g_k has a different k dependence than $G_k^{\alpha\beta}$ [Eq. (A4)] the quantity J_{av} of (A11) is not exactly equal to J even if $G_{ij}^{\alpha\beta}$ and J_{ij} are confined to closest intersublattice neighbors. However, calculations show that the difference between J_{av} and J is less than 1% and thus negligible.

The numerical values shown in Eqs. (23) and (45) are obtained by using the standard expressions for λ_k , μ_k , and $\tilde{\omega}_k = \omega_k(1+c)$ for a two-sublattice Heisenberg antiferromagnet (see, for example, Ref. 2) together with $G_k^{\alpha\beta}$ given by Eq. (32) for the rutile structures and⁷

$$G_k^{\alpha\beta} = 2G(\cos k_x a - \cos k_y a) \quad (\text{A12})$$

for cubic RbMnF₃. Sums were computed on a CDC 6600 over $n=10^6$, 2.5×10^6 , and 8×10^6 points in the Brillouin zone (advantage was taken of symmetries) and the results, which fell on a straight line when plotted versus $1/n$, were extrapolated to $n=\infty$. Equations (23) are valid to first order in J_1 and J_3 . Higher-order terms are completely negligible for the relatively small values of $Z_1 J_1 / Z_2 J_2$ and $Z_3 J_3 / Z_2 J_2$ encountered here.

APPENDIX B: INACCURACY OF $\tilde{\chi}(\vec{q}, T)$ IN THE CRITICAL REGION

In the paramagnetic phase, A/A_∞ and $\langle \omega \rangle$ are numerically calculated using the approximant $\hat{\chi}(\vec{q}, T)$ as given by RF. As $T \rightarrow T_c(T_N)$, errors develop in the results such that the calculated pair correlations $\langle \tilde{S}_i \cdot \tilde{S}_j \rangle$ of Eq. (35) become noticeably smaller than the more reliable values obtained from high-temperature series expansions and there is an increasing violation of the required sum rule,

$$\Gamma = \frac{1}{N} \sum_{\vec{q}} \langle \tilde{S}_{\vec{q}} \cdot \tilde{S}_{-\vec{q}} \rangle / S(S+1) = \frac{1}{N} \sum_{\vec{q}} \hat{\chi}(\vec{q}, T) = 1. \quad (\text{B1})$$

This behavior is quite clearly displayed in Table IV where, for the bcc lattice, the spin dependences of the nearest-neighbor correlation and Γ in the critical region are shown. In the second column are listed the critical nearest-neighbor correlations $\langle \frac{1}{2} \frac{1}{2} \frac{1}{2} \rangle_c^{\text{ser}}$ as obtained by RF from extrapolations of the high-temperature series expansions to the critical temperature T_c ; this same correlation $\langle \frac{1}{2} \frac{1}{2} \frac{1}{2} \rangle_c^{\text{app}}$, obtained from Eq. (35) using the $\hat{\chi}(\vec{q}, T)$, is given in the next column. The remaining columns show the calculated Γ of Eq. (B1) for the temperatures T_c and $1.4T_c$, respectively.

For the $S=\infty$ case, the results are in good agreement with predictions. The nearest-neighbor correlations agree to within 5% (in fact, the agreement at T_c is quite good for all S) and the sum rule (B1) is well satisfied. For $S=\frac{5}{2}$, (B1) is still fairly well obeyed; however, for the smaller S the sum rule rapidly breaks down, with Γ becoming appreciably less than unity for $T \rightarrow T_c$. This causes the calculated A/A_∞ and $\langle \omega \rangle$ to become, respectively, less than and greater than their "true" values.

The errors do not result from the numerical computations since increasing the number of points in the \vec{q} -space summation has little effect on the results; the problem must therefore arise from the nature of the $\hat{\chi}(\vec{q}, T)$ approximant. RF show that, at the critical point, $\hat{\chi}(\vec{q}, T)$ takes the form [see Eqs. (6.1) and (7.1) of Ref. 22]

TABLE IV. Spin dependences of the critical nearest-neighbor correlation $\langle \frac{1}{2} \frac{1}{2} \frac{1}{2} \rangle_c^{\text{ser}}$ obtained from extrapolations of high-temperature series expansions, the same correlation $\langle \frac{1}{2} \frac{1}{2} \frac{1}{2} \rangle_c^{\text{app}}$ obtained from the approximant $\hat{\chi}(\vec{q}, T)$, and the calculated sum Γ of Eq. (B1) for the temperatures T_c and $1.4T_c$.

Spin	$\langle \frac{1}{2} \frac{1}{2} \frac{1}{2} \rangle_c^{\text{ser}}$	$\langle \frac{1}{2} \frac{1}{2} \frac{1}{2} \rangle_c^{\text{app}}$	$\Gamma(T_c)$	$\Gamma(1.4T_c)$
∞	0.273	0.259	0.995	0.996
$\frac{5}{2}$	0.263	0.250	0.960	0.989
$\frac{3}{2}$	0.254	0.242	0.929	0.980
1	0.240	0.229	0.878	0.964
$\frac{1}{2}$	0.199	0.190	0.729	0.908

$$\hat{\chi}(\vec{q}, T) \approx \hat{D} / [K^2(\vec{q})a_0^2]^{1-\eta/2}, \quad (\text{B2})$$

where

$$K^2(\vec{q}) = (6/a_0^2) [1 - \cos(\frac{1}{2}q_x a) \cos(\frac{1}{2}q_y a) \cos(\frac{1}{2}q_z a)]$$

for the bcc lattice, with lattice constant a and nearest-neighbor distance a_0 , [$K^2(\vec{q}) \sim q^2$ for $q \rightarrow 0$]. RF further show that the \vec{q} -independent \hat{D} varies for the different S (and also for different lattice structures) but that η is spin independent and, thus, there is *no* way that the sum rule of (B1) can be satisfied for *all* S . In addition, RF point out that the $\hat{\chi}(\vec{q}, T)$ is designed, and has been numerically optimized, to give the best results for small qa (or, equivalently, for large r_{ij}), whereas A/A_∞ and $\langle \omega \rangle$ are heavily weighted by the near-neighbor correlations.

This effect may not be so important in light of the relatively good agreement between the two independent values for the nearest-neighbor correlations, even at T_c . (Other near-neighbor correlations show similar agreements between the two methods.)

To correct for the effects of the sum-rule violation on A/A_∞ , we divide our numerical result for the first term in Eq. (29) by the calculated value of Γ and add the remaining terms in $\langle \frac{1}{2} \frac{1}{2} \frac{1}{2} \rangle$, using values obtained from Eq. (35), to the result. This procedure brings the corrected value of A/A_∞ into better agreement with the "true" value, especially at T_c where the result can be compared with an alternative more accurate determination of A/A_∞ . The corrected value for $\langle \omega \rangle$ is then obtained by forming the ratio of Eq. (33) to the corrected A/A_∞ .

*Work supported by the U. S. Atomic Energy Commission.

¹P. A. Fleury, S. P. S. Porto, L. E. Cheesman, and H. J. Guggenheim, *Phys. Rev. Lett.* **17**, 84 (1966); P. A. Fleury, S. P. S. Porto, and R. Loudon, *Phys. Rev. Lett.* **18**, 658 (1967).

²P. A. Fleury and R. Loudon, *Phys. Rev.* **166**, 514 (1968).

³P. A. Fleury, *Phys. Rev.* **180**, 591 (1969).

⁴S. R. Chinn and H. J. Zeiger, *Phys. Rev. Lett.* **21**, 1589 (1968); P. A. Fleury, J. M. Worlock, and H. J. Guggenheim, *Phys. Rev.* **185**, 738 (1969); P. A. Fleury, *J. Appl. Phys.* **41**, 886 (1970); S. R. Chinn, H. J. Zeiger, and J. R. O'Connor, *J. Appl. Phys.* **41**, 894 (1970); P. A. Fleury and H. J. Guggenheim, *Phys. Rev. Lett.* **24**, 1346 (1970).

⁵Y. R. Shen and N. Bloembergen, *Phys. Rev.* **143**, 372 (1966); Y. R. Shen, *J. Appl. Phys.* **38**, 1490 (1967); T. Moriya, *J. Appl. Phys.* **39**, 1042 (1968).

⁶R. J. Elliott, M. F. Thorpe, G. F. Imbusch, R. Loudon, and J. B. Parkinson, *Phys. Rev. Lett.* **21**, 147 (1968).

⁷R. J. Elliott and M. F. Thorpe, *J. Phys. C* **2**, 1630 (1969).

⁸P. S. Pershan and A. Oseroff, *Phys. Rev. B* **1**, 2359 (1970).

⁹T. Kawasaki, *J. Phys. Soc. Jap.* **29**, 1144 (1970).

¹⁰J. S6lyom, *Z. Phys.* **243**, 382 (1971); *Proceedings of the Second International Conference on Light Scattering in Solids*, edited by M. Balkanski (Flammarion, Paris 1971), p. 165.

¹¹R. W. Davies, S. R. Chinn, and H. J. Zeiger, *Phys. Rev. B* **4**, 992 (1971); S. R. Chinn, R. W. Davies, and H. J. Zeiger, *Phys. Rev. B* **4**, 4017 (1971); R. W. Davies, *Phys. Rev. B* **5**, 4598 (1972).

¹²M. G. Cottam, *Solid State Commun.* **10**, 99 (1972); *J. Phys. C* **5**, 1461 (1972); *Solid State Commun.* **11**, 889 (1972).

¹³C. R. Natoli and J. Ranninger, *J. Phys. C* **6**, 323 (1973); *J. Phys. C* **6**, 345 (1973); *J. Phys. C* **6**, 370 (1973); *J. Phys. C* **6**, 386 (1973).

¹⁴W. J. Brya, R. R. Bartkowski, and P. M. Richards, *AIP Conf. Ser.* **5**, 339 (1972).

¹⁵W. J. Brya, P. M. Richards, and R. R. Bartkowski, *Phys. Rev. Lett.* **28**, 826 (1972).

¹⁶W. J. Brya, P. M. Richards, and P. A. Fleury, *AIP Conf. Proc.* **10**, 729 (1973).

¹⁷A. Okazaki, K. C. Turberfield, and R. W. H. Stevenson, *Phys. Lett.* **8**, 9 (1964).

¹⁸O. Nikotin, P. A. Lindgard, and O. W. Dietrich, *J. Phys. C* **2**, 1168 (1969).

¹⁹See, for example, C. P. Slichter, *Principles of Magnetic Resonance* (Harper and Row, New York, 1963), pp. 226-230.

²⁰M. Buchanan, W. J. L. Buyers, R. J. Elliott, R. T. Harley, W. Hayes, A. M. Perry, and I. D. Saville, *J. Phys. C* **5**, 2011 (1972).

²¹G. S. Rushbrooke and P. J. Wood, *Mol. Phys.* **1**, 257 (1958).

²²D. S. Ritchie and M. E. Fisher, *Phys. Rev. B* **5**, 2668 (1972).

²³See, for example, R. A. Tahir-Kheli and D. ter Haar, *Phys. Rev.* **127**, 88 (1962).

²⁴M. E. Fisher and R. J. Burford, *Phys. Rev.* **156**, 583 (1967).

²⁵V. Jaccarino and R. G. Shulman, *Phys. Rev.* **107**, 1196 (1957); P. Heller and G. B. Benedek, *Phys. Rev. Lett.* **8**, 428 (1962); G. G. Low, *Proc. Phys. Soc. Lond.* **82**, 992 (1963).

²⁶A complete magnetization curve for MnF_2 , which combines the results of Ref. 25, may be found in F. Keffer, in *Handbuch der Physik*, edited by S. F. Flügge (Springer, Berlin, 1966), Vol. 18, p. 127.

²⁷L. P. Kadanoff *et al.*, *Rev. Mod. Phys.* **39**, 395 (1967).

²⁸The previously reported (Ref. 14) agreement between experiment and theory for the behavior of A/A_∞ in the paramagnetic state was fortuitous since the multispin decoupling procedure used there was not as accurate as the results of Eqs. (27); however, we now obtain considerably better agreement for the first moment $\langle \omega \rangle$ than obtained earlier.

²⁹Recent measurements in the antiferromagnetic perovskite RbCoF_3 [J. Nouet, D. J. Toms, and J. F. Scott, *Phys. Rev. B* **7**, 4874 (1973)] also show a large increase in A_∞/A_0 over the prediction of Eq. (21); possible effects of the unquenched Co^{2+} orbital momentum on the theoretical results should, however, be considered.

³⁰C. S. Windsor and R. W. H. Stevenson, *Proc. Phys. Soc. Lond.* **87**, 501 (1966).

³¹M. T. Hutchings, M. F. Thorpe, R. J. Birgeneau,

- P. A. Fleury, and H. J. Guggenheim, Phys. Rev. B 2, 1362 (1970).
- ³²P. M. Richards and W. J. Brya, Phys. Rev. B (to be published).
- ³³C. Satoko, J. Phys. Soc. Jap. 28, 1367 (1970).
- ³⁴J. H. Van Vleck, Phys. Rev. 74, 1168 (1948).
- ³⁵R. W. Davies, Phys. Rev. B 5, 4598 (1972).
- ³⁶T. Oguchi, Phys. Rev. 117, 117 (1960).